Supplementary Information for

"Automated Quantification of Stereotypical Motor Movements in Autism Using Persistent Homology"

Contents

Supplementary Note 1. Data Information

Supplementary Table S1. Overall SMM statistics in our dataset calculated using manual video annotation.

Participant	Sessions		No. of Bouts			Duration of Bouts (min)		
	No.	Dur. (min)	Rock	Flap	Flaprock	Rock	Flap	Flaprock
STUDY 1								
1	2	50.2	52	2	57	5.2	0.2	4.9
2	2	32.1	1	209	0	0.1	8.1	0
3	2	64.5	1	52	28	0.1	2.9	2.4
4	2	38.9	55	70	0	12.7	6.2	0
5	2	44.7	12	75	17	1.2	8.6	1.6
6	2	55.8	112	0	9	31.3	0	1.6
STUDY 2								
1	3	49.8	77	57	64	7.4	6.5	5
2	2	51.1	77	33	1	7.7	1	0.1
3	2	75.9	1	18	0	0.02	0.5	0
4	3	87.5	46	38	0	13.2	2	0
5	2	55.2	68	11	6	10.9	1.3	0.3
6	1	25.3	64	0	6	20.2	0	6

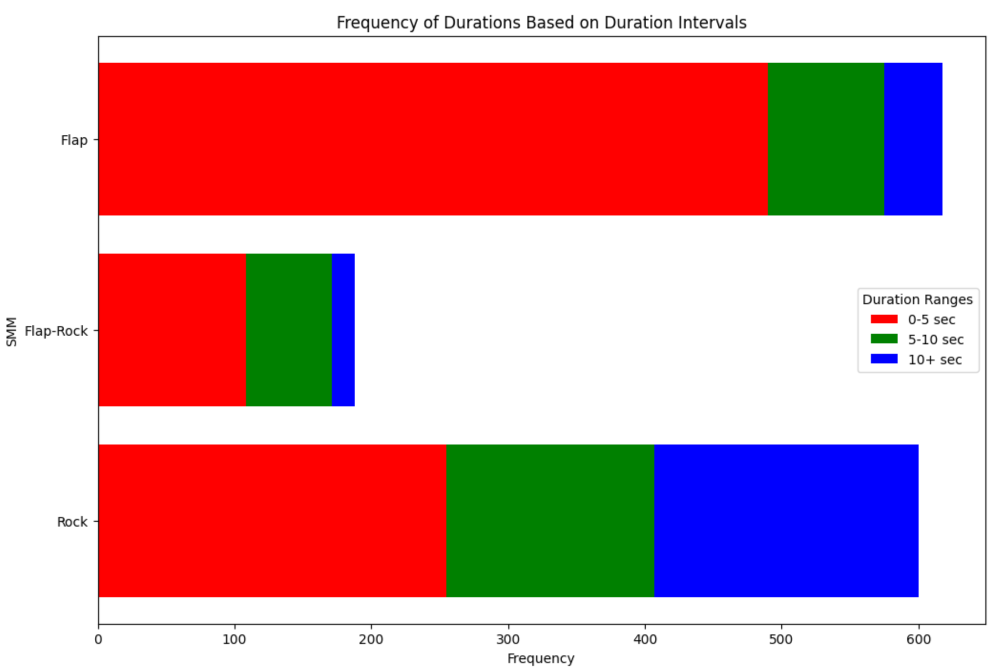

Supplementary Figure S1. Displays the distribution of SMM durations, grouped into time bins. The majority of flapping and flap-rock behaviors occur in short bursts lasting 0–5 seconds, whereas rocking behaviors are more evenly distributed across the 0–5, 5–10, and 10+ second intervals. This suggests for this dataset that rocking tends to manifest in more sustained episodes compared to flapping-related movements, which are typically brief and transient.

Supplementary Note 2. YOLOv5 Training

We trained a YOLOv5l model via transfer learning. In other words, a pre-trained model of YOLOv5 trained on the COCO[1] dataset is adapted to our custom dataset while still leveraging the model's prior knowledge allowing for a more efficient learning process. A carefully chosen 2,500 video frames were manually annotated by drawing bounding boxes around the person of interest, ensuring we saw the people in an even distribution of situations and poses so tracking would be as accurate as possible. We used an 80/10/10 (train/test/validation) split. Cropping, blurring, and vertical flipping augmentations were applied to the training data to simulate new training examples from which the model could learn. Below shows the results of training the model:

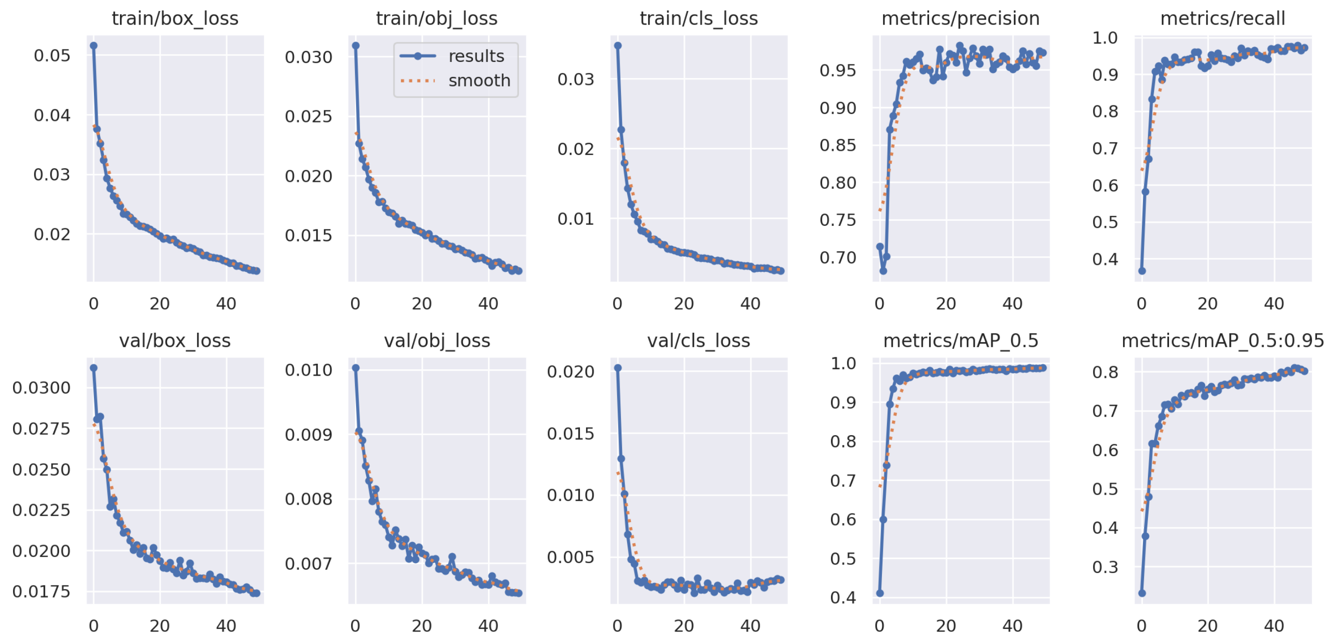

Supplementary Figure S2. YOLOv5l Model Performance Results.

Supplementary Note 3. Persistent Homology

The goal of persistent homology is to determine the underlying shape $\mathbb{X}$ given a finite, discrete sample X. If a time series is periodic, then its sliding window point cloud X is homotopy equivalent to S^1 (circular)[2]. The primary method to analyze these high-dimensional point clouds is via persistent homology. However, to understand homology, one needs to understand what a simplicial complex is:

Definition 1 (Simplicial Complex)**.** *A simplicial complex is a collection K of nonempty sets such that:*

- *if $\sigma \in K$, then $0 < \#(\sigma) < \infty$*
- *if $\sigma \in K$ and $\varnothing \neq \tilde{\sigma} \subset \sigma$, then $\tilde{\sigma} \in K$*

We call σ an n-simplex and denote $K^{(n)}$ the collection of n-simplices.

A 0-simplex represents a vertex; a 1-simplex represents an edge that connects two vertices; a 2-simplex represents a triangle, and analogous interpretations for higher dimensions. Homology, a concept from algebraic topology, is then used to describe the properties of a simplicial complex. These properties include the number of connected components (intuitively, distinct clusters or groups of connected masses), 1-dimensional holes (closed loops bounding empty space), 2-dimensional voids (enclosed shells or surfaces), and higher-dimensional analogues. Let n-chains, denoted as $C_n(K;\mathbb{F})$, be the field $\mathbb{F}$ vector space generated by the n-simplices of a simplicial complex K. That is

$$C_n(K;\mathbb{F}) = span_{\mathbb{F}}(K^{(n)})$$

The n-chains form a chain complex

$$C_n \xrightarrow{\delta_{n-1}} C_{n-1} \rightarrow \cdots \xrightarrow{\delta_1} C_1 \xrightarrow{\delta_0} C_0$$

where δ_i is the boundary map given by

$$\delta_i(\sigma) = \sum_{i=0}^{n} (-1)^i (\sigma / \{x_i\}) \in C_{n-1}$$

for $\sigma \in C_n(K)$. The boundary map satisfies $\delta_n \circ \delta_{n+1} = 0 \ \forall n \in \mathbb{N}$.

Definition 2 (Simplicial Homology Group)**.** *The n^{th} homology group of K is denoted as*

$$H_n(K) = \frac{\ker \delta_n}{\operatorname{im} \delta_{n+1}}$$

The homology of a topological space X consists of a sequence of these vector spaces $H_n(X)$. The rank of $H_n(X)$ counts the number of n-dimensional holes. For example, $dim(H_0(X))$ counts the number of connected components, and $dim(H_1(X))$ counts the number of loops.

In practice, we can construct a simplicial complex, known as a *Vietoris-Rips complex*, to compute features on sets of discrete data points.

Definition 3. *Given a metric space $(X, \mathbf{d}_X)$, the Vietoris-Rips complex (Rips complex) is defined as:*

$$R_\alpha(X) = \{\, \sigma \subset X \mid 0 < \#(\sigma) < \infty\,, \, \mathsf{diam}(\sigma) \leq \alpha \,\}$$

where $\#(\sigma)$ is the cardinality of σ and diam(σ) is the diameter of σ.

Persistent homology tracks the evolution of topological features of complexes such as $R_\alpha(X)$, as the scale parameter α increases. More formally, this is called a *Rips filtration*

Definition 4. *Given a metric space $(X, \mathbf{d}_X)$, the Rips Filtration is defined as:*

$$\mathscr{R}(X) = \left\{ i_{\alpha',\alpha} : R_\alpha(X) \hookrightarrow R_{\alpha'}(X) \right\}_{0 < \alpha \leq \alpha'}$$

Thus, we obtain a set of sub-complexes of our Rips complex

$$\emptyset \subseteq R_{\alpha_0}(X) \subseteq R_{\alpha_1}(X) \subseteq \cdots \subseteq R_{\alpha_n}(X)$$

Applying homology to each sub-complex in the filtration induces linear maps between vector spaces in each dimension n:

$$H_n(R_{\alpha_0}(X)) \to H_n(R_{\alpha_1}(X)) \to \cdots \to H_n(R_{\alpha_n}(X))$$

This structure is known as persistent homology $PH_n(X)$, which tracks how n-dimensional features appear and disappear across distance scales. Each topological feature corresponds to an interval $[b_i, d_i)$, representing the distance scale at which the topological feature is created and when it disappears. The multi-set of such intervals is the barcode or persistence diagram, providing a summary of the dataset's multiscale topological structure.

Supplementary Figure S3. Effect of Sliding Window Point Cloud Dimension d on Persistent Homology

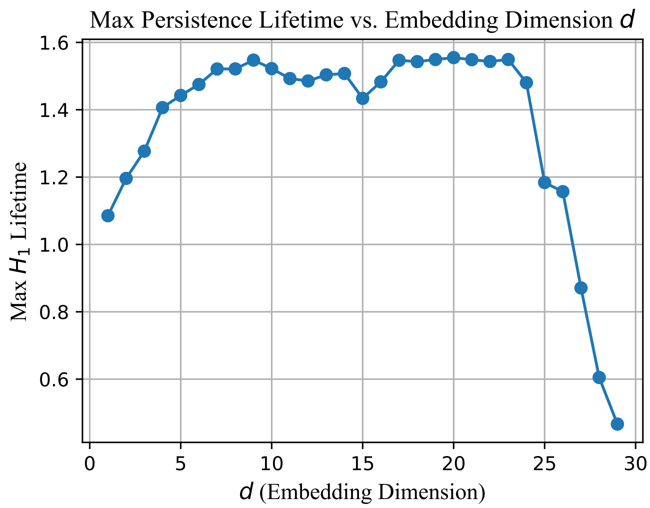

Supplementary Figure S3. Max H_1 lifetime of $S\mathbb{W}$ embedding of time series shown in Figure 7 of the manuscript across different ambient dimensions.

Supplementary Note 4. Accelerometer Data

In order to directly compare results from prior studies and test our *ATSM-SW1PerS* pipeline on a dataset with more temporal resolution, we used the same available data as the videos[3]. Aside from the video data, during both studies, participants wore three 3-axis accelerometers on each wrist and on the torso. Different accelerometers were used in each study. Study 1 used MITes 3-axis sensors recording ±2 g data at 60 Hz. Study 2 used Wockets 3-axis sensors recording ±4 g data at 90 Hz. Recordings were done across multiple sessions within each study. These readings serve as a high-resolution signal to test and benchmark our data analysis pipeline. To ensure consistency, each sensor was resampled to 95Hz, and the remainder of the pipeline, from detrending each signal component to computing the periodicity, mostly stays the same with the exception of the period estimation.

Estimating Period

In our main manuscript, we estimate the period of a 2-dimensional time series via the Complex Discrete Fourier Transform. However, this does not completely work for the 3-dimensional accelerometer time series. To accurately estimate the period of the entire system, we referred to a recently proposed framework: Learned Accurate Periodic Dictionaries (LAPIS), to estimate the period of multivariate time series[4]. Their method uses a Ramanujan Periodic Dictionary, which consists of structured, periodic basis functions with integer-valued periods. This dictionary provides a sparse and interpretable way to model periodicity, especially in noisy or incomplete signals that are more than 2-dimensional. A complete explanation of methods can be found in their paper and our implementation on GitHub, which offers a robust, and interpretable way to estimate the period of 3-dimensional accelerometer time series $F(t) = (f_x(t), f_y(t), f_z(t))$.

Supplementary Note 5. Bayesian Optimization

Bayesian Optimization was employed as a strategy to optimize expensive-to-evaluate functions such as optimal feature selection and hyperparameter tuning. Rather than doing a exhaustive grid search across all different combinations within the search space, Bayesian Optimization builds a probabilistic surrogate model to guide the search towards more promising regions.

Surrogate Model

The surrogate model, typically a Gaussian Process (GP), provides a probabilistic approximation of the objective function $f(\theta)$, where θ represents the features and hyper-parameters (the different Mediapipe landmarks and model hyperparameters). A Gaussian Process is defined as:

$$f(\theta) \sim \mathcal{GP}\left(m(\theta), k(\theta, \theta')\right),$$

where:

- $m(\theta)$ is the mean function, often assumed to be zero,
- $k(\theta, \theta')$ is the kernel that encodes the similarity between different parameter settings.

Acquisition Function

An acquisition function $a(\theta)$ is used to decide where to sample next, balancing searching uncertain regions of the search space with refining known good areas. One common acquisition function is the Expected Improvement (EI), defined as:

$$\mathrm{EI}(\theta) = \mathbb{E}\left[\max(f(\theta) - f(\theta^+), 0)\right],$$

where $f(\theta^+)$ is the best observed value so far.

Optimization Process

The Bayesian Optimization algorithm proceeds as follows:

1. **Initialization:** Evaluate the objective function $f(\theta)$ at a few initial points $\{\theta_i\}_{i=1}^n$ to construct the initial surrogate model. We did 30 random starts to build the surrogate model.
2. **Model Update:** Fit or update the Gaussian Process using the current set of observations $\{(\theta_i, f(\theta_i))\}$.
3. **Acquisition Optimization:** Maximize the acquisition function to select the next hyperparameter setting:
$$\theta_{n+1} = \arg\max_{\theta} a(\theta).$$
4. **Evaluation:** Evaluate $f(\theta_{n+1})$ using the actual expensive objective (e.g., F1 score for Random Forest).
5. **Iteration:** Repeat steps 2–4 until a certain number of iterations. We saw after 200 iterations, our evaluations did not improve much, so we set that as our limit.

This approach significantly reduces the number of evaluations required to identify near-optimal hyperparameters, which is particularly beneficial when each evaluation is computationally expensive. For all model training across experiments, we saw using 200 function evaluations and 30 random initializations consistently indicated that retaining all available landmarks led to optimal performance. So when doing any other training, it would make sense to only explore model hypperparametrs, which will reduce the amount of iterations required. One could do 25 random starts and 100 iterations only exploring hyperparametrs drastically reducing optimization time. The parameter space and implementation can be found in our GitHub.

Supplementary Note 6. Computational Resources

For fast processing of videos, we utilized Northeastern University's Explorer HPC cluster. For data analysis, processing each video and landmarks can be done in parallel, thus we leveraged SLURM-based job arrays. We split the computations into two parts, video processing and data analysis, each requiring one node. The MediaPipe inference stage used a NVIDIA V100 GPU; the average runtime with these specifications for a single video was approximately 15 minutes. For the data analysis stage, we process 12 landmarks in parallel that require at least 12 CPU cores. To improve efficiency in other computations, we allocated 36 CPU cores and 60GB of memory, with a maximum wall time of 1 hour. On average, each feature extraction would be completed within 5-15 minutes (when using a step size of $1/fps$). When doing a step size of 4 seconds, this time reduces to 1-5 minutes.

Supplementary Table S2. Experiment 1 - Stratified Set Classification

Supplementary Table S2. Classification performance of Random Forest models using PS_{10} and PS_1 periodicity scores across binary and multiclass settings.

	Pose Estimation				Accelerometer				Accelerometer + Period			
Class	Precision	Recall	F1	Support	Precision	Recall	F1	Support	Precision	Recall	F1	Support
PS_{10} - Binary Classification												
None	0.83	0.95	0.88	449	0.89	0.95	0.92	511	0.91	0.93	0.92	511
SMM	0.91	0.72	0.80	319	0.93	0.86	0.89	396	0.91	0.88	0.89	396
Weighted $F1$				**0.85**				**0.91**				**0.91**
PS_1 - Binary Classification												
None	0.81	0.92	0.86	449	0.89	0.87	0.88	511	0.91	0.89	0.90	511
SMM	0.86	0.70	0.77	319	0.84	0.86	0.85	396	0.86	0.88	0.87	396
Weighted $F1$				**0.82**				**0.87**				**0.89**
PS_{10} - Multiclass Classification												
None	0.80	0.92	0.86	449	0.89	0.94	0.91	511	0.91	0.93	0.92	511
Rock	0.87	0.78	0.82	259	0.93	0.86	0.89	299	0.92	0.89	0.91	299
Flap	0.22	0.09	0.13	43	0.68	0.72	0.70	65	0.74	0.77	0.75	65
Flap-Rock	0.50	0.12	0.19	17	0.75	0.56	0.64	32	0.76	0.59	0.67	32
Weighted $F1$				**0.79**				**0.88**				**0.89**
PS_1 - Multiclass Classification												
None	0.81	0.92	0.86	449	0.90	0.85	0.87	511	0.91	0.88	0.89	511
Rock	0.90	0.77	0.83	259	0.87	0.76	0.81	299	0.90	0.85	0.88	299
Flap	0.09	0.07	0.08	43	0.38	0.63	0.48	65	0.57	0.78	0.66	65
Flap-Rock	0.00	0.00	0.00	17	0.22	0.34	0.27	32	0.54	0.69	0.60	32
Weighted $F1$				**0.79**				**0.80**				**0.86**

Supplementary Table S3. Experiment 2 - Leave-One-Session-Out

Supplementary Table S3. Comparison of our $\mathbb{SW}1PerS$ model trained on accelerometer data (RF-PS_1 (Accel) ; RF-PS_{10} (Accel)), combining frequency-domain features (RF-$PS_1 + Period$ (Accel), RF-$PS_{10} + Period$ (Accel)), and the pose skeleton (RF-PS_1 (Pose) ; RF-PS_{10} (Accel)), using a Random Forest classifier against prior work. Performance is evaluated using Accuracy (A) and weighted F_1 score, the latter being more informative under class imbalance.

Study	Method	S1		S2		S3		S4		S5		S6		Mean	
		F_1	A	F_1	A	F_1	A	F_1	A	F_1	A	F_1	A	F_1	A
Study 1	SVM[3]	0.73	0.86	0.36	0.85	0.50	0.94	0.73	0.67	0.44	0.75	0.46	0.87	0.54	0.82
	RF-RQA[5]	—	0.71	—	0.73	—	0.70	—	0.92	—	0.68	—	0.94	—	0.78
	CNN-Rad[6]	0.70	0.71	0.74	0.70	0.69	0.68	0.92	0.78	0.68	0.78	0.93	0.78	0.78	0.74
	Frequency-domain CNN[7]	**0.97**	**0.99**	0.78	**0.89**	**0.94**	**0.99**	**0.96**	**0.97**	**0.96**	**0.98**	**0.99**	**0.98**	**0.93**	**0.97**
	RF-$PS_{10} + Period$ (Accel)	0.90	0.90	**0.94**	**0.94**	**0.94**	0.95	0.95	0.95	0.90	0.91	0.92	0.92	**0.93**	0.93
	RF-$PS_1 + Period$ (Accel)	0.90	0.90	0.91	0.91	**0.94**	0.94	0.92	0.92	0.87	0.88	0.93	0.93	0.91	0.91
	RF-PS_{10} (Accel)	0.89	0.89	**0.94**	**0.94**	**0.94**	0.94	0.95	0.95	0.90	0.91	0.90	0.90	0.92	0.92
	RF-PS_{10} (Pose)	0.78	0.81	0.68	0.75	0.68	0.76	0.77	0.78	0.70	0.77	0.88	0.87	0.75	0.79
	RF-PS_1 (Accel)	0.88	0.88	0.81	0.83	0.92	0.93	0.88	0.89	0.78	0.81	0.92	0.92	0.87	0.88
	RF-PS_1 (Pose)	0.78	0.80	0.68	0.74	0.72	0.78	0.79	0.79	0.68	0.74	0.86	0.86	0.75	0.79
Study 2	SVM	0.43	0.71	0.26	0.79	0.03	0.99	0.86	0.90	0.72	0.73	—	—	0.46	0.82
	RF-RQA	—	0.80	—	0.69	—	0.99	—	0.95	—	0.85	—	—	—	0.856
	CNN-Rad	0.67	0.68	0.22	0.02	0.02	0.77	0.75	0.75	0.68	0.75	0.80	0.49	0.41	0.58
	Frequency-domain CNN	**0.96**	**0.97**	**0.95**	**0.98**	**0.85**	**1.00**	**0.98**	**0.99**	**0.94**	**0.97**	—	—	**0.94**	**0.98**
	RF-$PS_{10} + Period$ (Accel)	0.85	0.85	0.60	0.58	—	—	0.96	0.96	0.70	0.70	**0.98**	**0.98**	0.82	0.81
	RF-$PS_1 + Period$ (Accel)	0.87	0.87	0.59	0.57	—	—	0.94	0.94	0.74	0.74	0.97	0.97	0.82	0.82
	RF-PS_{10} (Accel)	0.83	0.83	0.62	0.61	—	—	0.93	0.93	0.71	0.71	**0.98**	**0.98**	0.81	0.81
	RF-PS_{10} (Pose)	0.83	0.84	0.71	0.75	—	—	0.96	0.96	0.86	0.86	**0.98**	**0.98**	0.87	0.88
	RF-PS_1 (Accel)	0.81	0.81	0.64	0.63	—	—	0.92	0.91	0.64	0.64	**0.98**	**0.98**	0.80	0.79
	RF-PS_1 (Pose)	0.83	0.85	0.71	0.76	—	—	0.96	0.96	0.86	0.86	0.95	0.95	0.86	0.88

Supplementary Table S4. Experiment 3 - Leave-One-Individual-Out

Supplementary Table S4. Binary classification performance (Weighted F_1 Scores) of pose trajectories vs. accelerometer signals per participant under Leave-One-Individual-Out evaluation.

Participant	Pose		Accelerometer			
	PS_1	PS_{10}	PS_1	PS_{10}	$PS_1 + Period$	$PS_{10} + Period$
1	0.81	0.81	0.83	0.85	0.87	0.85
2	0.71	0.71	0.68	0.68	0.65	0.66
3	0.72	0.68	0.92	0.94	0.94	0.94
4	0.89	0.88	0.92	0.96	0.92	0.96
5	0.79	0.79	0.74	0.82	0.81	0.82
6	0.89	0.91	0.94	0.93	0.93	0.90
Mean	**0.80**	**0.80**	**0.84**	**0.86**	**0.85**	**0.86**

Experiment Figures

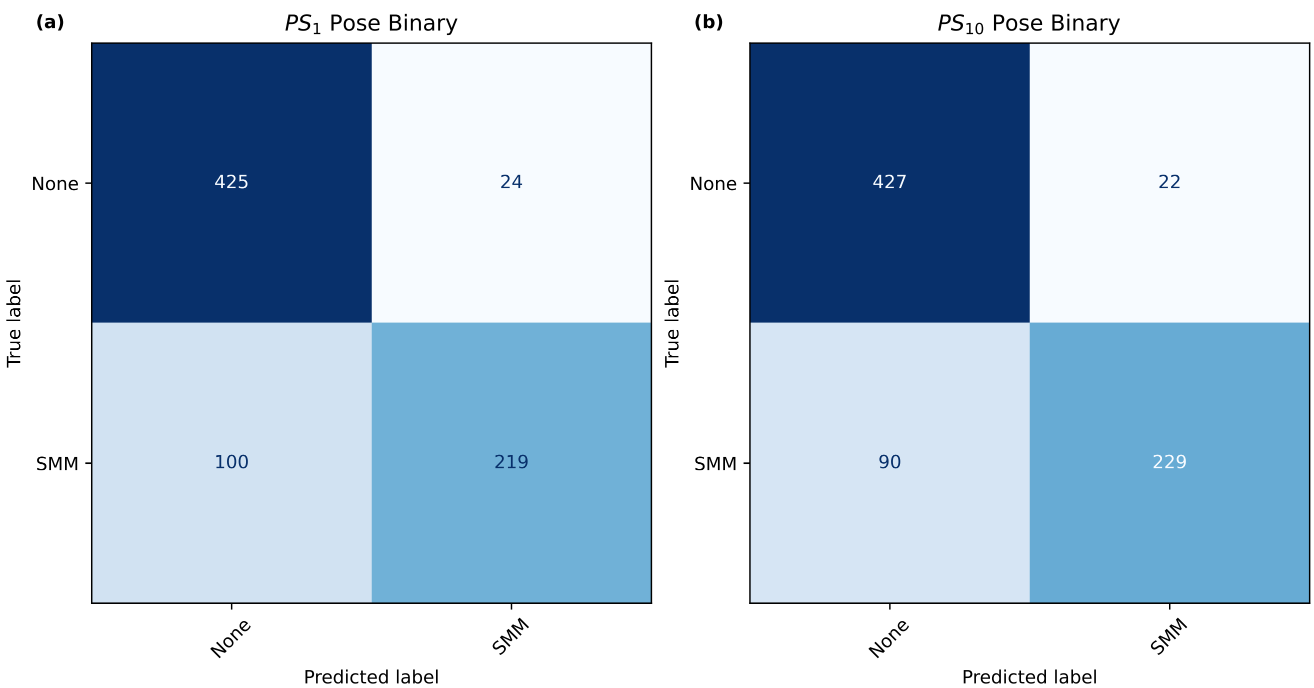

Supplementary Figure S4. Experiment 1 confusion matrices showing binary model's performance using pose-based landmarks. We see both PS_1 (a), and $PS_{10}(b)$ have similar performance even though we have an order of magnitude less information using PS_1 scores. It is important to note that our model rarely hallucinates periodicity which is important in clinical settings.

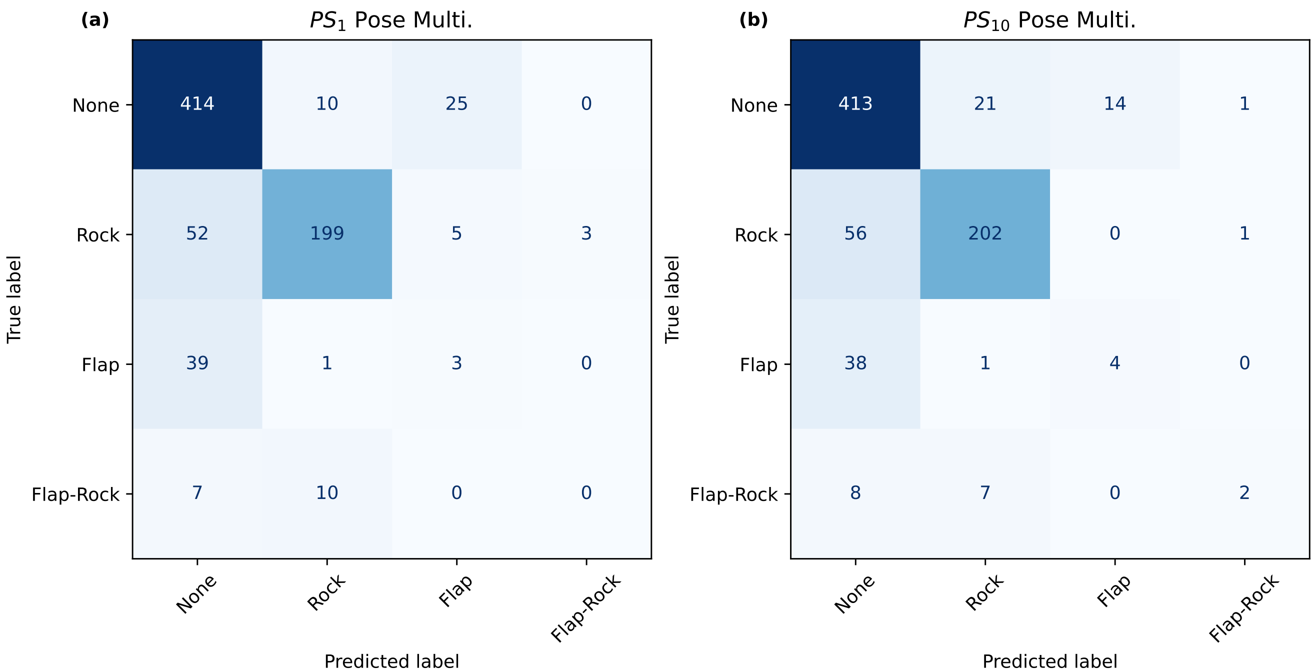

Supplementary Figure S5. Experiment 1 confusion matrices showing multiclass model's performance using pose-based landmarks. Both PS_1 (a), and $PS_{10}(b)$ have similar performance. For both panels, we see that near all of flapping instances are misclassified as no stereotypy.

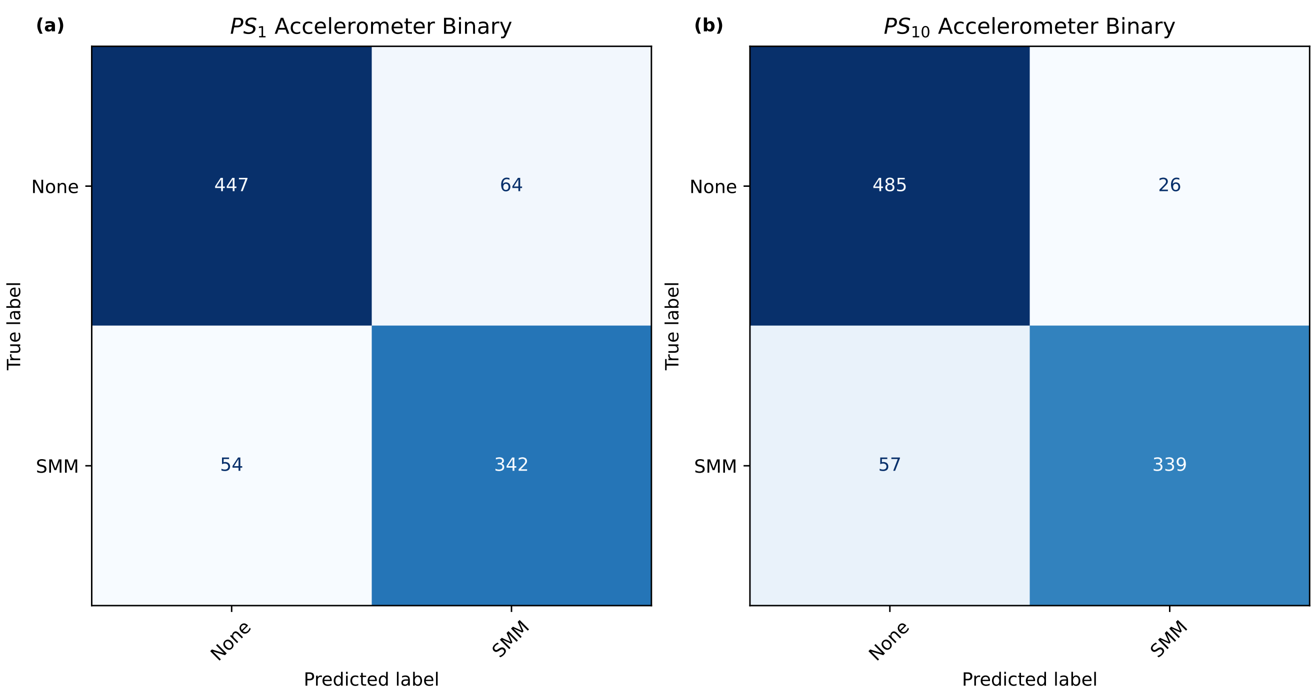

Supplementary Figure S6. Experiment 1 confusion matrices showing binary model's performance using accelerometer-based sensors. We again see both PS_1 (a), and $PS_{10}(b)$ have similar performance.

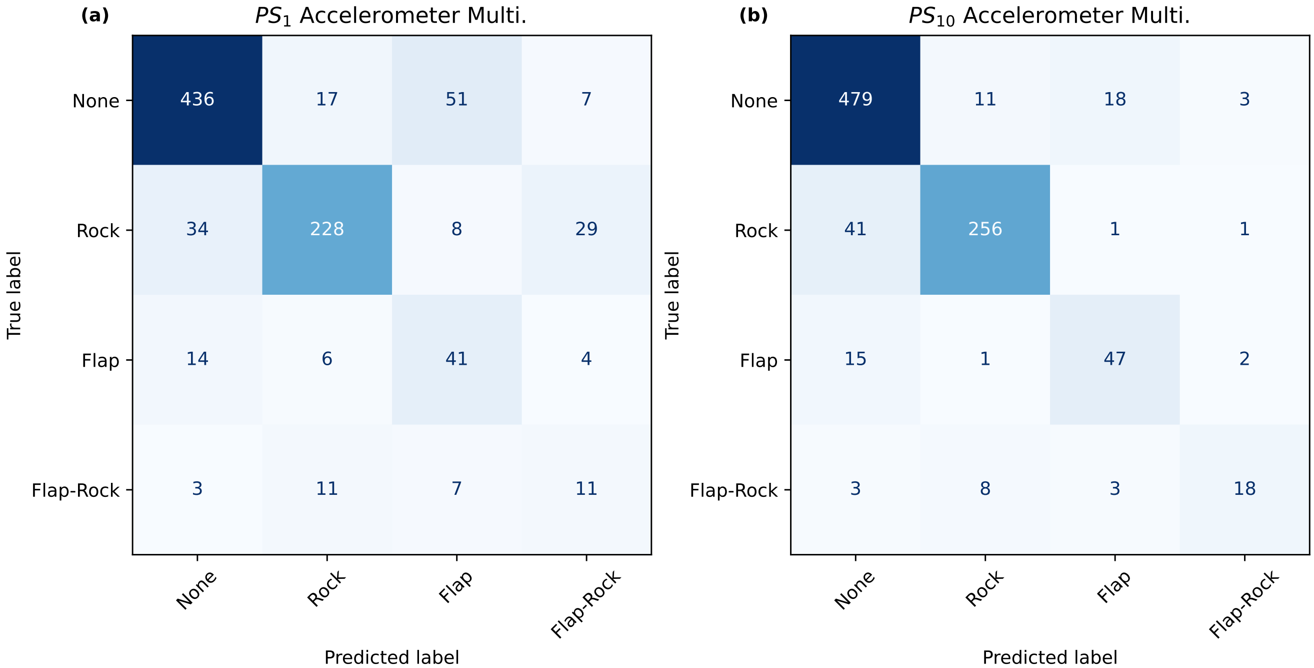

Supplementary Figure S7. Experiment 1 confusion matrices showing multiclass model's performance using accelerometer-based sensors. Both PS_1 (a), and $PS_{10}(b)$ have similar performance. For both panels, we see the model's ability to detect repetitive flapping motions is much better than using pose-based landmarks. This is likely due to accelerometers not being affected by occlusions.

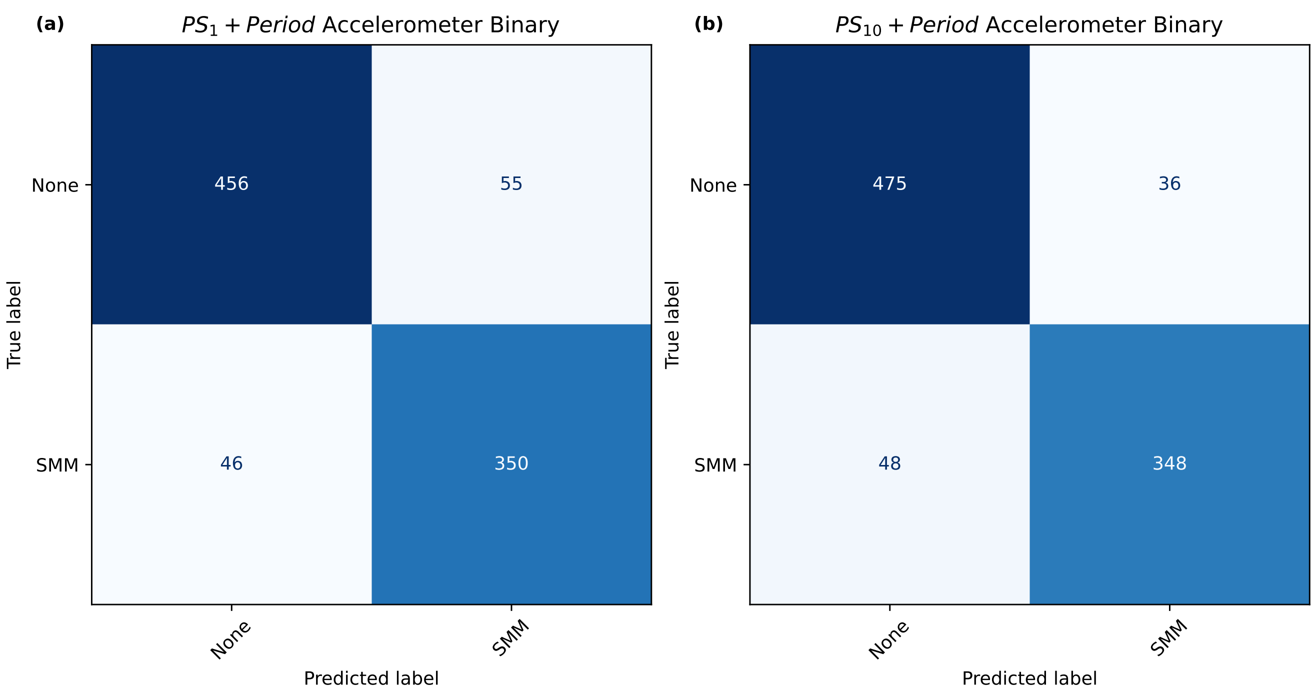

Supplementary Figure S8. Experiment 1 confusion matrices showing binary model's performance using accelerometer-based sensors using frequency-domain and our periodicity scores.

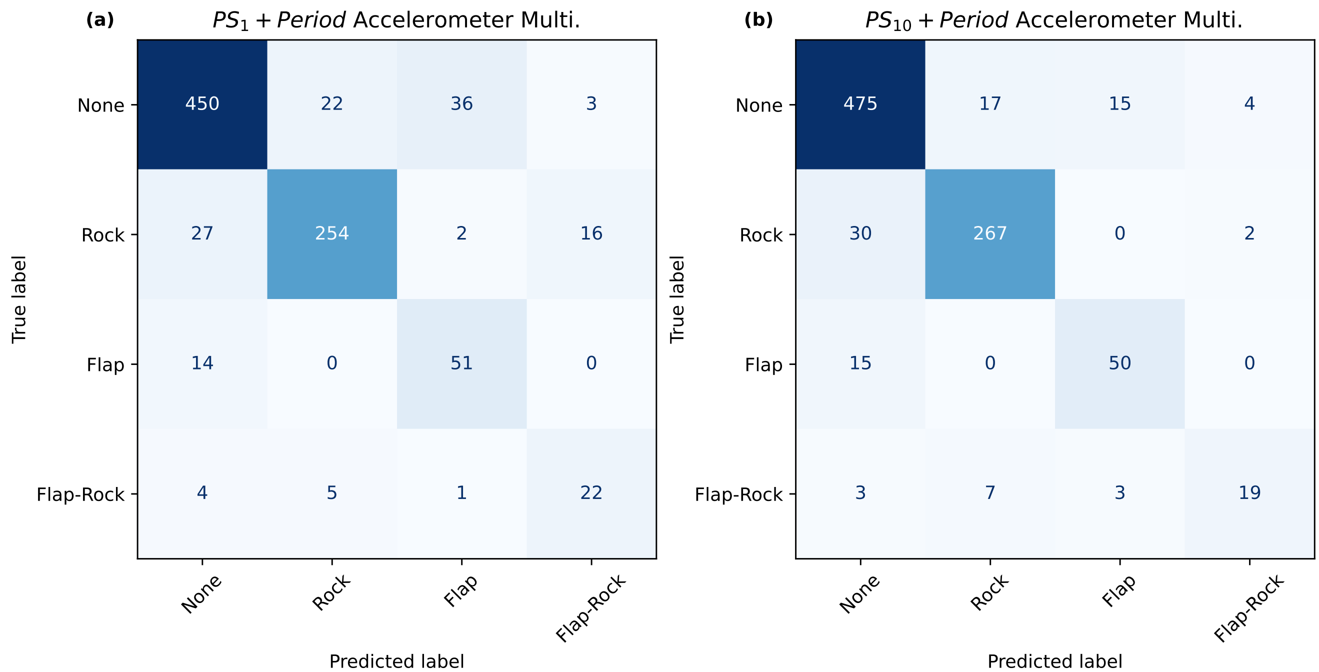

Supplementary Figure S9. Experiment 1 confusion matrices showing multiclass model's performance using accelerometer-based sensors using frequency-domain and our periodicity scores.

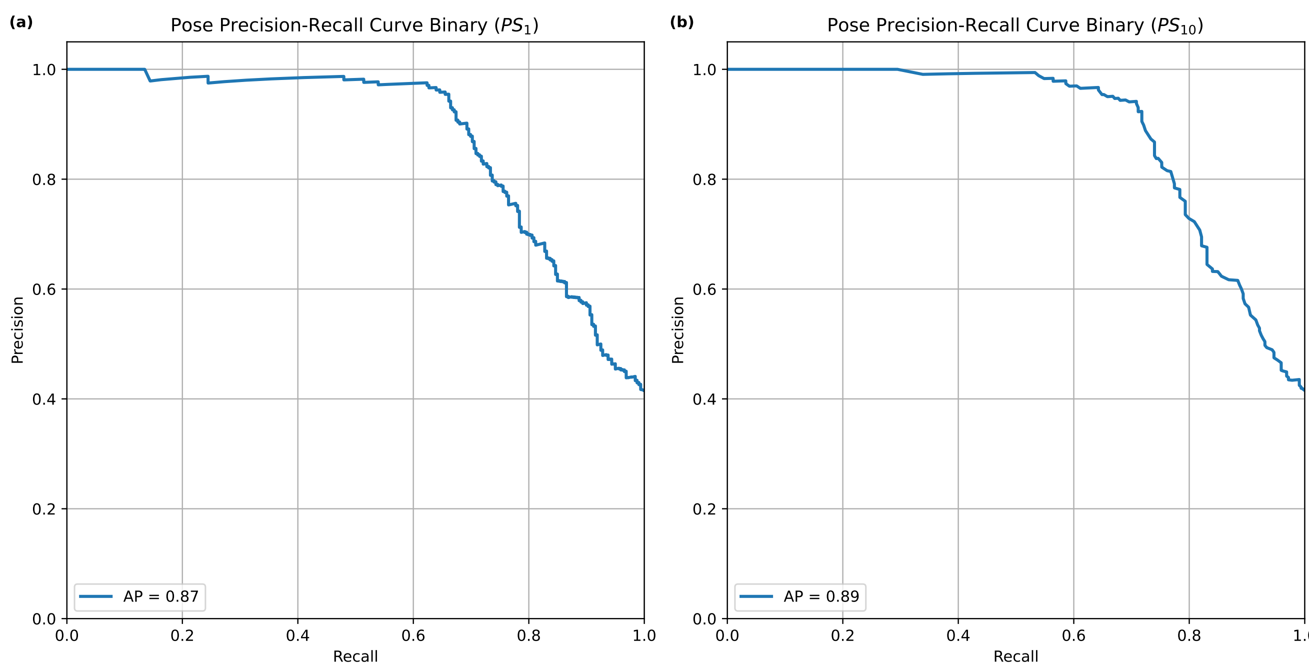

Supplementary Figure S10. Experiment 1 binary classification precision–recall curves for each periodicity score method using pose-based landmarks. Panel a shows results for the PS_1 model (AP = 0.87), while panel b displays the PS_{10} model (AP = 0.89). Both curves reflect the trade-off between recall and precision across decision thresholds, with high average precision (AP) indicating strong separability between classes.

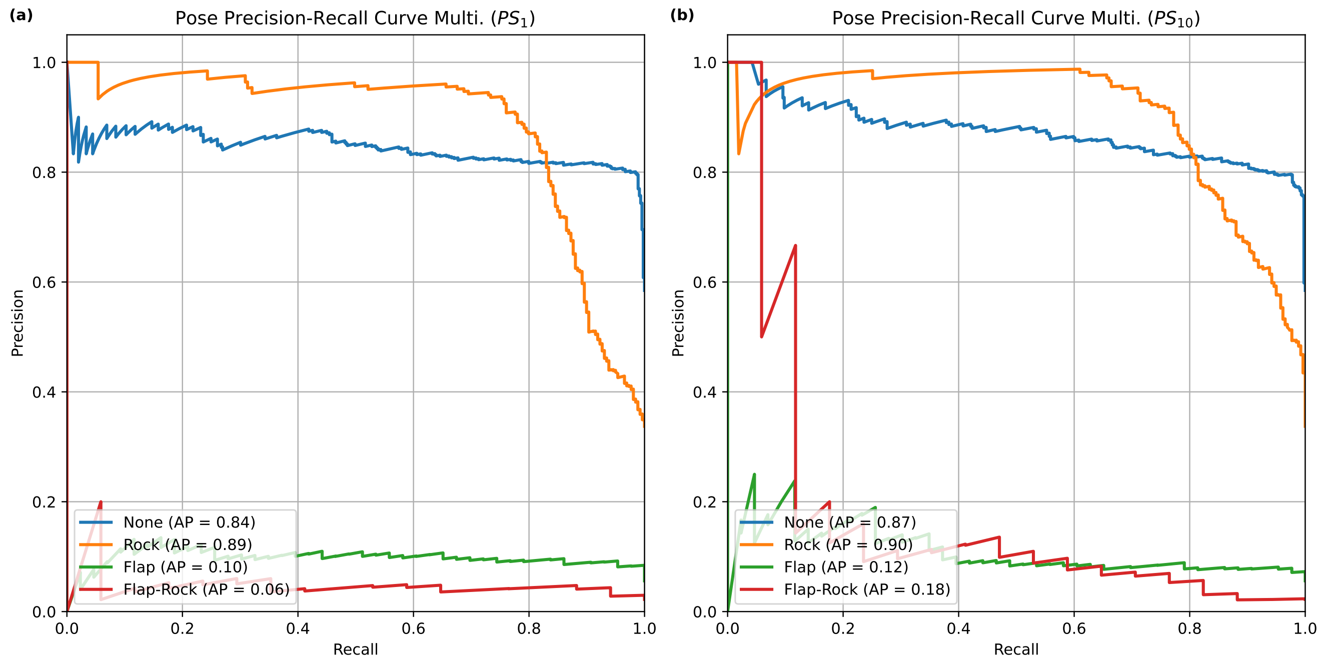

Supplementary Figure S11. Experiment 1 multiclass classification precision–recall curves for each periodicity score method using pose-based landmarks.

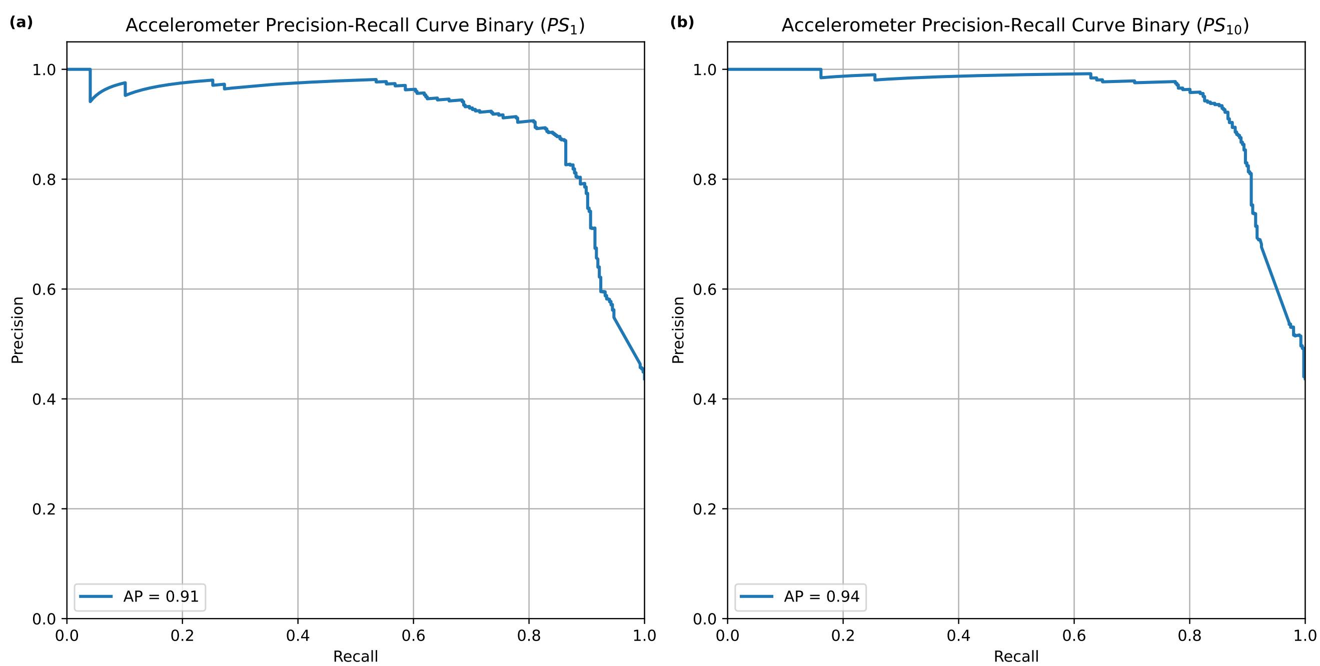

Supplementary Figure S12. Experiment 1 binary classification precision–recall curves for each periodicity score method using accelerometer-based sensors. Panel (a) shows results for the PS_1 model (AP = 0.91), while panel (b) displays the PS_{10} model (AP = 0.94). Both curves show that using the accelerometer-based sensors slightly increases performance over the pose-based landmarks.

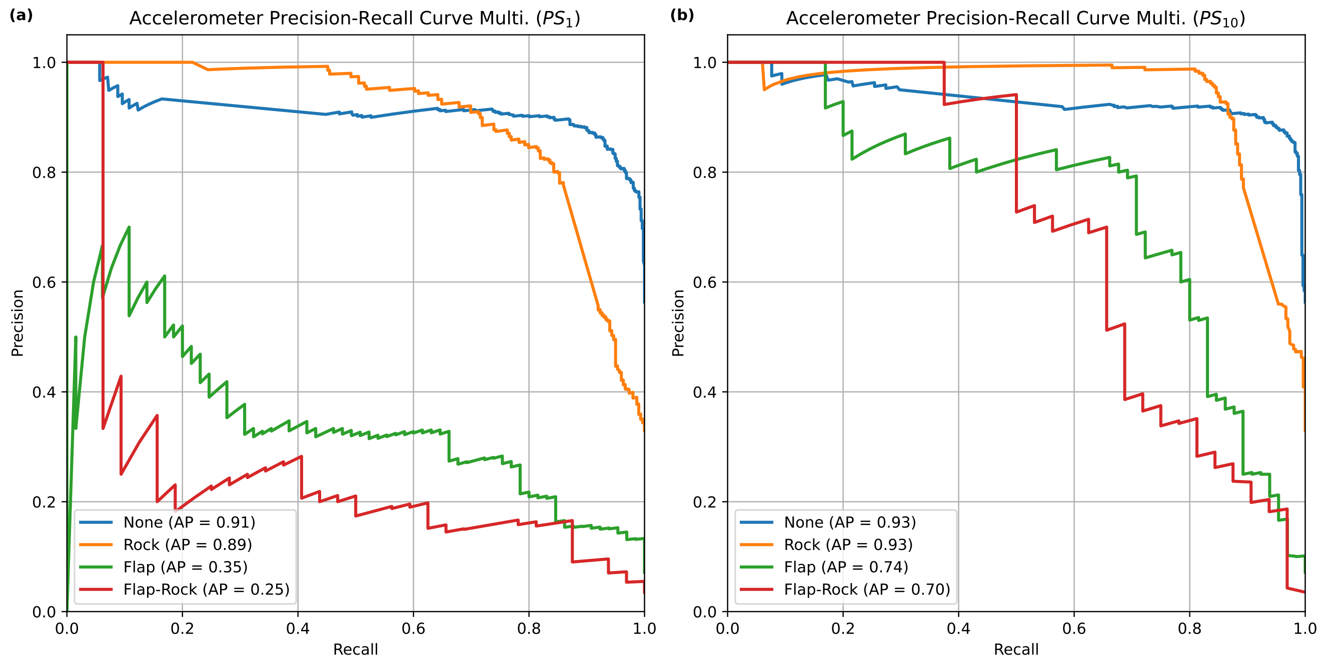

Supplementary Figure S13. Experiment 1 multiclass classification precision–recall curves for each periodicity score method using accelerometer-based sensors.

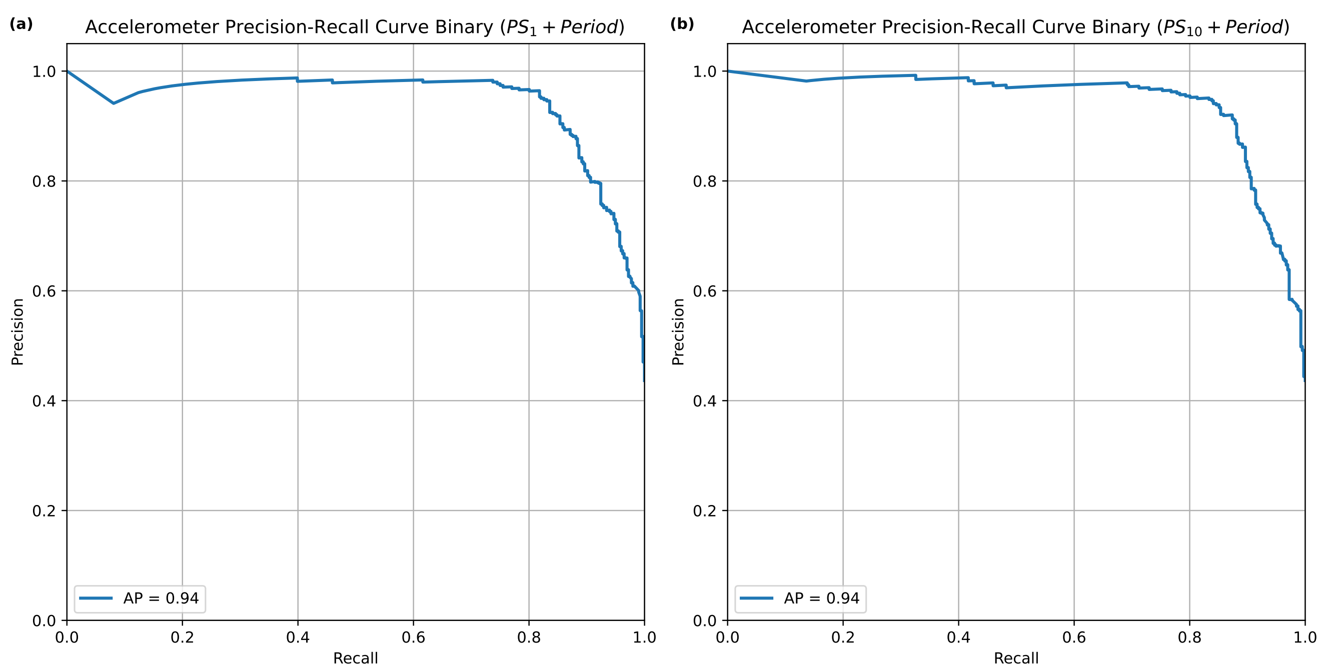

Supplementary Figure S14. Experiment 1 binary classification precision–recall curves for each periodicity score method using accelerometer-based sensors.

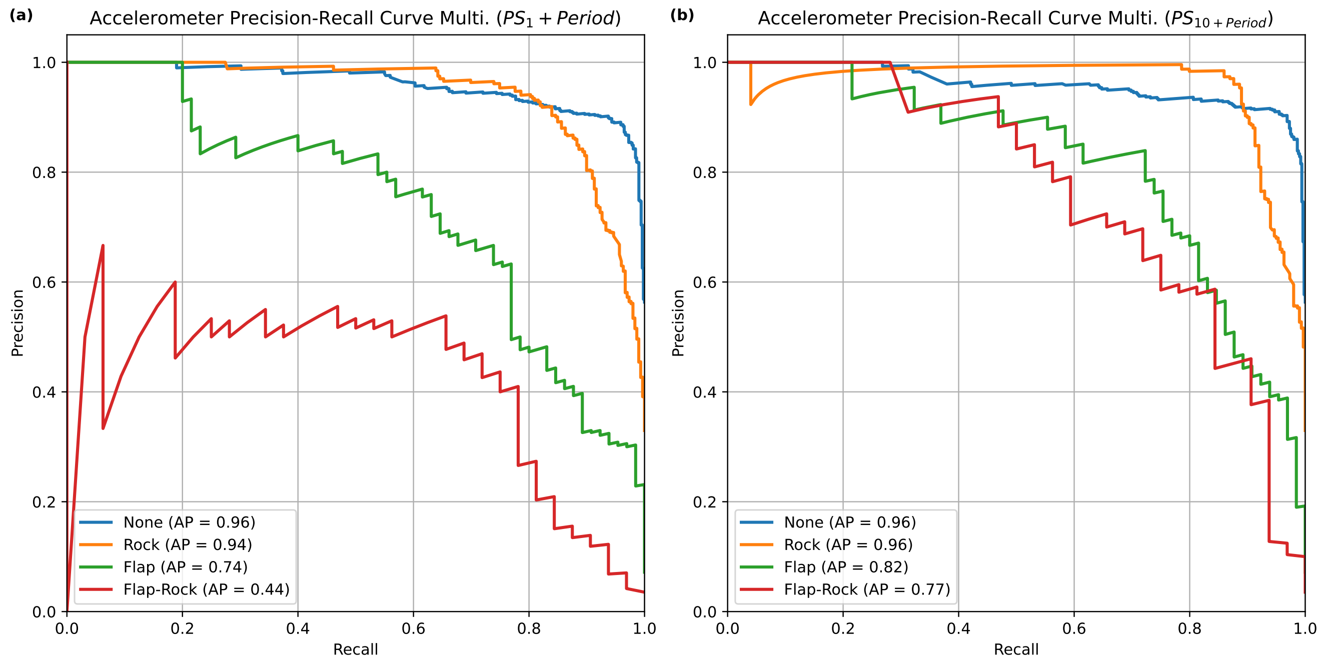

Supplementary Figure S15. Experiment 1 multiclass classification precision–recall curves for each periodicity score method combined with frequency-domain features using accelerometer-based sensors.

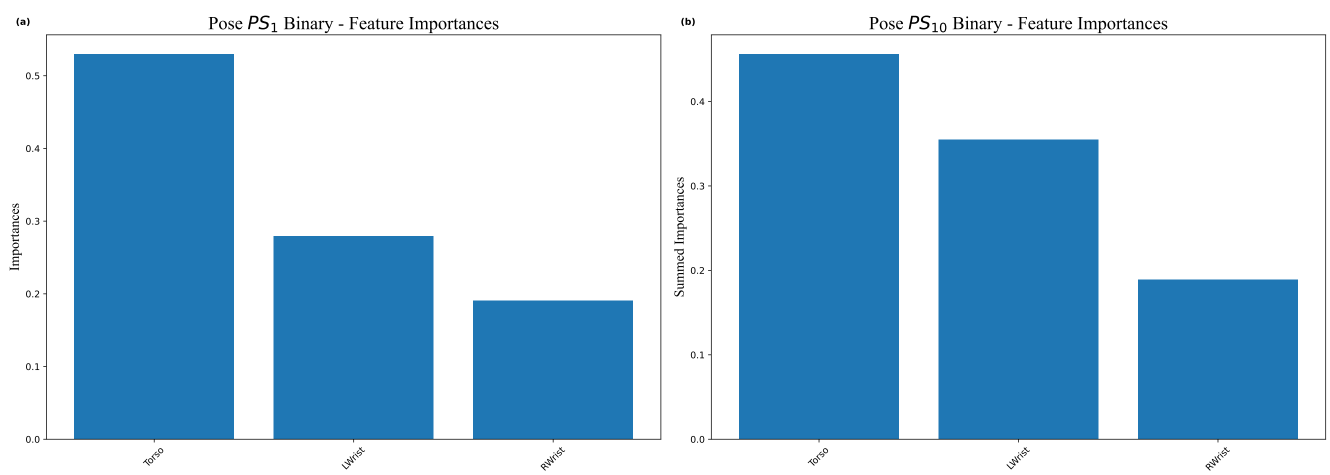

Supplementary Figure S16. Experiment 1 feature importances for binary classification using accelerometer-based sensors. Panel (a) shows Torso contributes the most to the model's decisions. In contrast, panel (b) reveals that all sensors have more equal contribution. This prominence in torso-related features aligns with the pose-based landmark feature importances and prior findings[5].

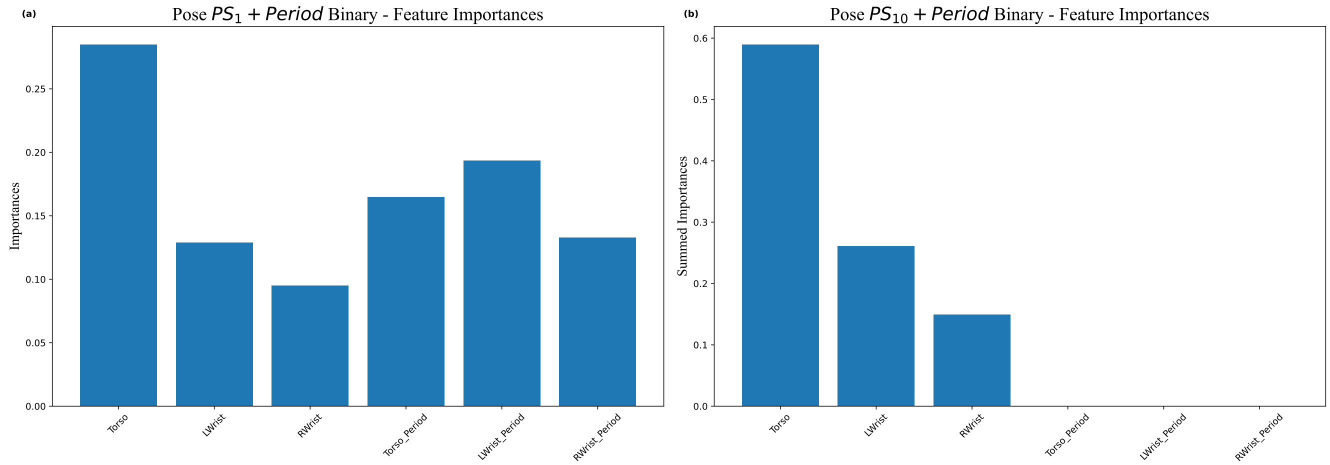

Supplementary Figure S17. Experiment 1 feature importances for binary classification using accelerometer-based sensors using both periodicity scores and period features. Panel (a) shows all features make a contribution to the model's decisions. This time, panel (b) shows that the Torso is primarily responsible in the full-resolution PS_{10} model.

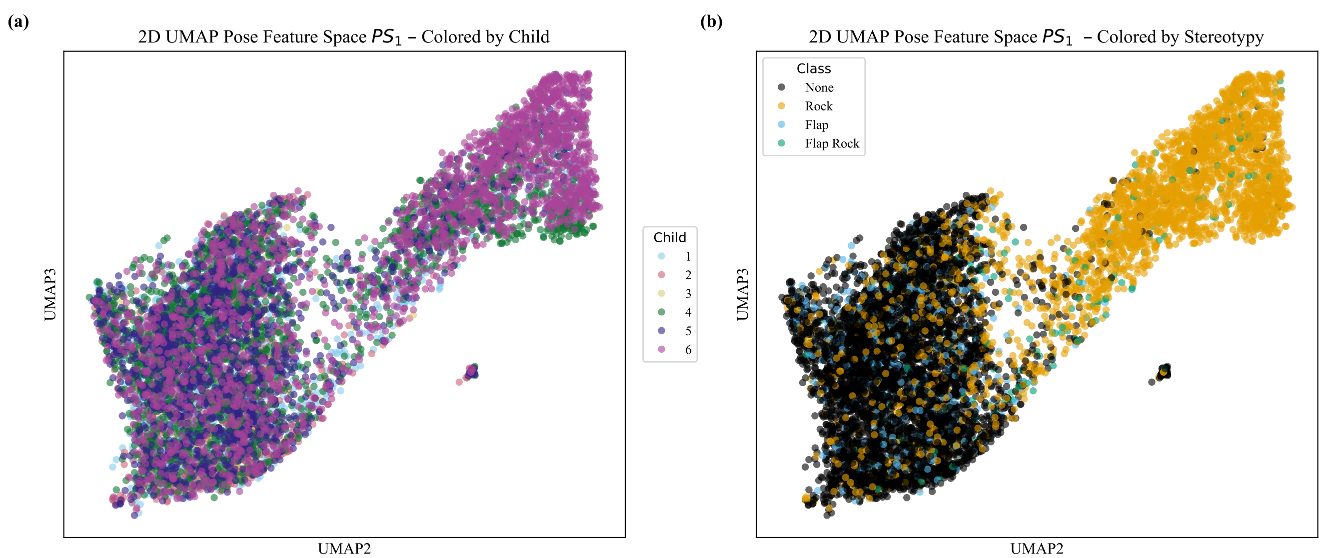

Supplementary Figure S18. Experiment 4 *UMAP* embeddings of pose-based landmark PS_1 feature space colored by (a) participant ID and (b) SMM class. Same organization as the rest

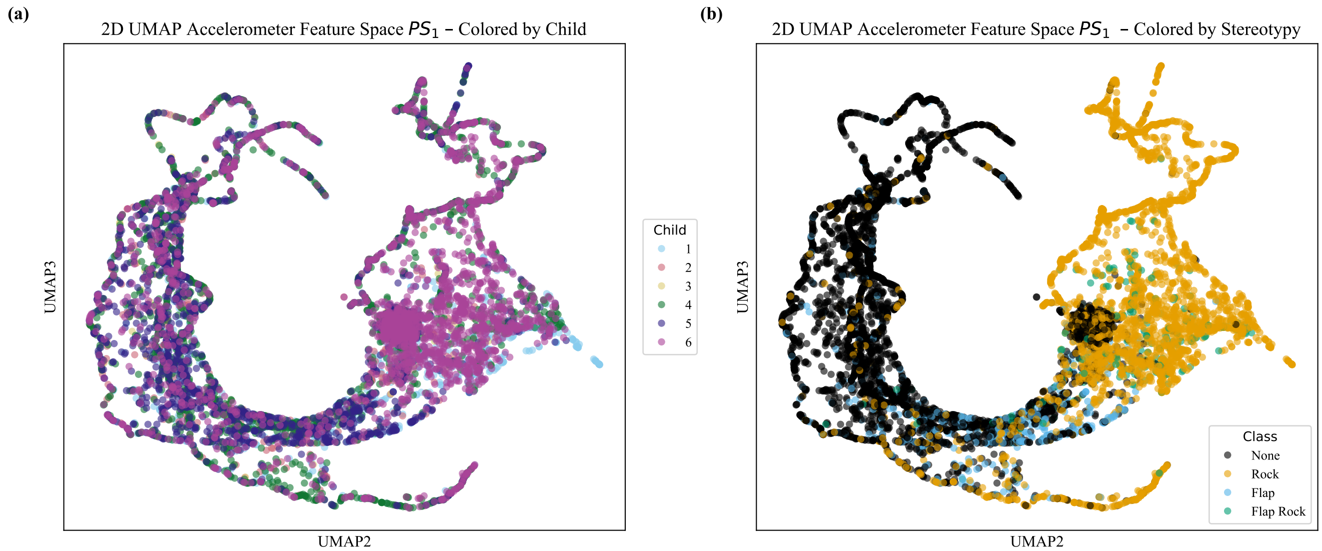

Supplementary Figure S19. Experiment 4 *UMAP* embeddings of accelerometer-based sensor PS_1 feature space colored by (a) participant ID and (b) SMM class. Note that the feature spaces are subsampled down for ease of visualization. In (a), the overlap across individuals suggests no variability based on ID. In contrast, (b) shows clear organization based on SMM class, indicating that despite individual variability, our topological features encode behaviorally meaningful patterns that generalize across participants even with accelerometer-based sensors so it is not specific to pose-based landmarks.

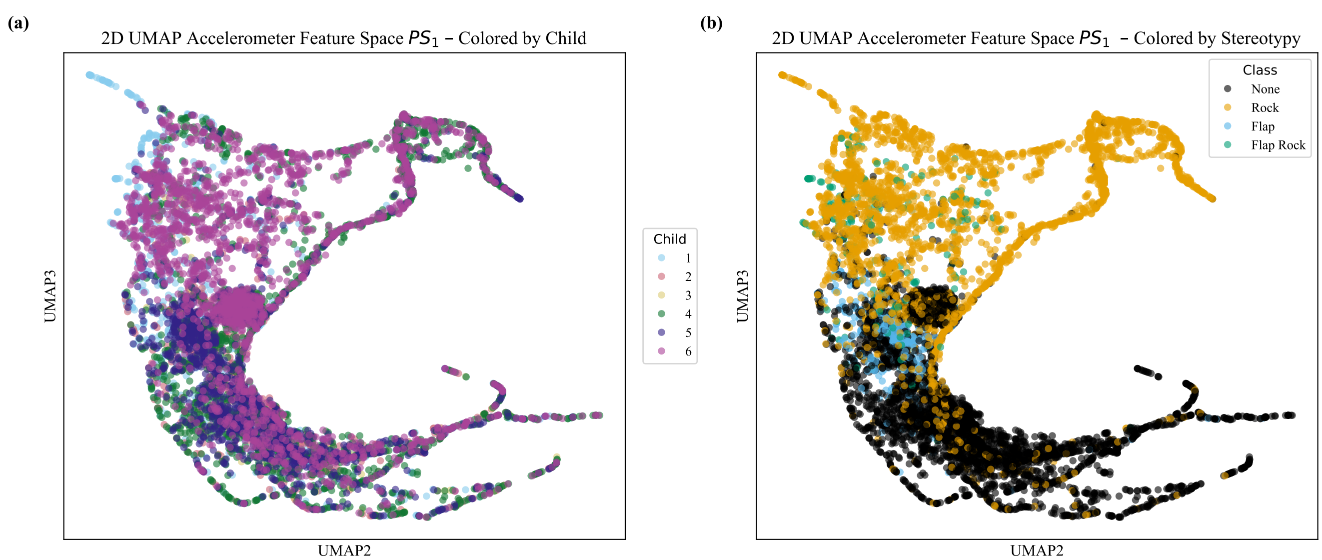

Supplementary Figure S20. Experiment 4 *UMAP* embeddings of accelerometer-based sensor PS_{10} feature space colored by (a) participant ID and (b) SMM class.

Supplementary Note 7. Application of Methods

Illustrative Example: Persistence Changes Within a Participant Over Time

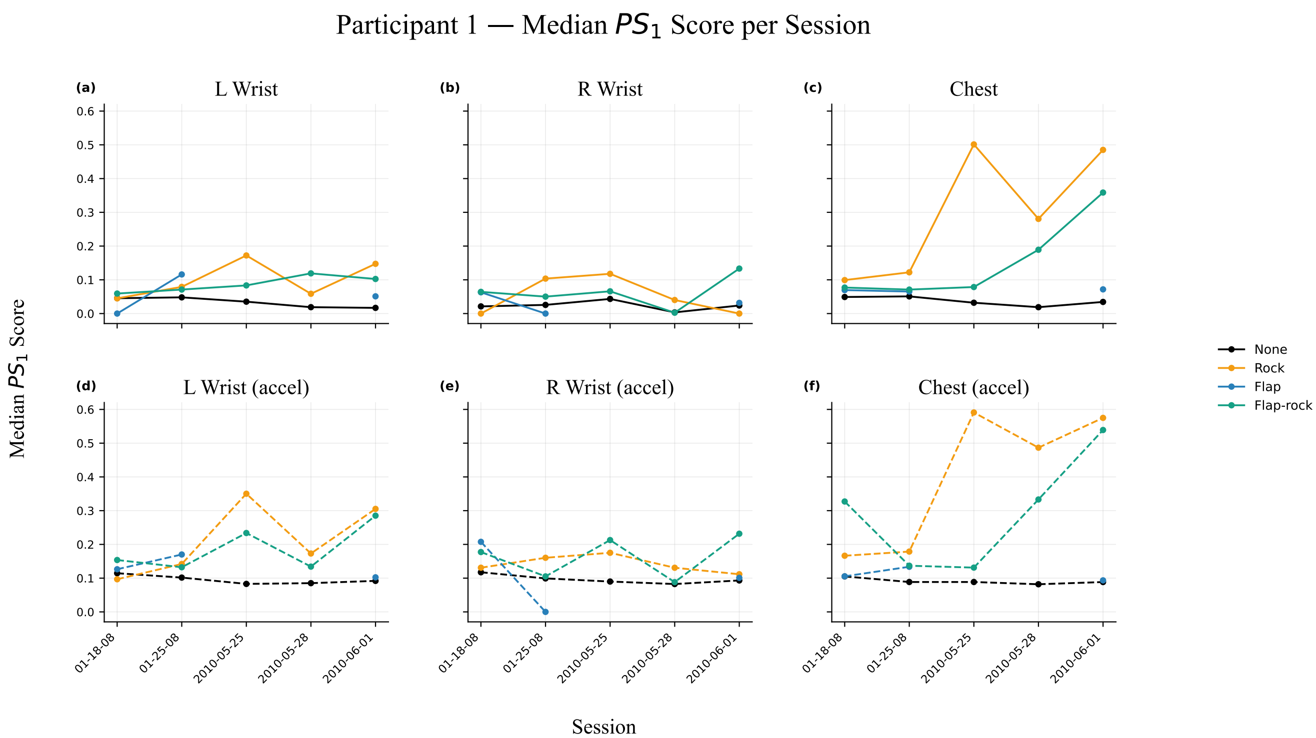

Supplementary Figure S21. Evolution of median PS_1 score derived from $S\mathbb{W}1PerS$ pipeline on representative set of pose landmarks.

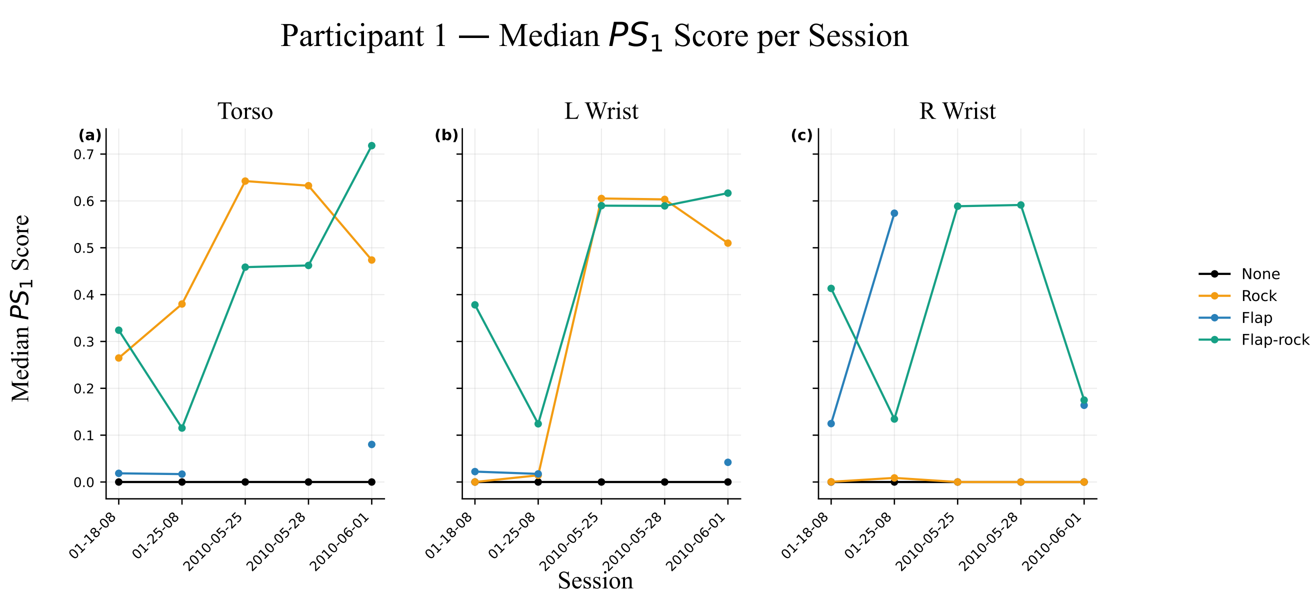

Supplementary Figure S22. Evolution of median PS_1 score derived from $S\mathbb{W}1PerS$ pipeline on accelerometer sensors

Periodicity Score Summary Across Participants, Sessions, and Annotations

Supplementary Table S5. Pose Landmarks Median ± SD PS_1 Scores per Sensor, Stratified by Participant, Session, and Annotation Part I

Participant	Session	Annotation	RWrist	LWrist	Chest	RWrist Accel	LWrist Accel	Chest Accel
1	01-18-08	None	0.021 ± 0.115	0.045 ± 0.109	0.049 ± 0.117	0.117 ± 0.116	0.115 ± 0.104	0.105 ± 0.104
		Rock	0.000 ± 0.109	0.045 ± 0.118	0.099 ± 0.153	0.131 ± 0.135	0.097 ± 0.113	0.166 ± 0.161
		Flap	0.063 ± 0.085	0.000 ± 0.001	0.070 ± 0.060	0.208 ± 0.058	0.126 ± 0.024	0.105 ± 0.081
		Flap-Rock	0.064 ± 0.099	0.059 ± 0.122	0.077 ± 0.119	0.177 ± 0.150	0.154 ± 0.146	0.327 ± 0.204
	01-25-08	None	0.026 ± 0.110	0.048 ± 0.101	0.051 ± 0.100	0.099 ± 0.101	0.102 ± 0.093	0.089 ± 0.087
		Rock	0.104 ± 0.179	0.079 ± 0.151	0.122 ± 0.170	0.160 ± 0.180	0.142 ± 0.109	0.179 ± 0.143
		Flap	0.000 ± 0.000	0.116 ± 0.157	0.065 ± 0.138	0.000 ± 0.089	0.170 ± 0.085	0.134 ± 0.084
		Flap-Rock	0.050 ± 0.100	0.071 ± 0.101	0.071 ± 0.127	0.105 ± 0.100	0.132 ± 0.113	0.137 ± 0.111
	05-25-10	None	0.043 ± 0.104	0.035 ± 0.111	0.032 ± 0.101	0.090 ± 0.090	0.083 ± 0.084	0.089 ± 0.084
		Rock	0.118 ± 0.145	0.172 ± 0.182	0.501 ± 0.256	0.175 ± 0.136	0.350 ± 0.177	0.591 ± 0.199
		Flap-Rock	0.066 ± 0.098	0.083 ± 0.086	0.079 ± 0.111	0.213 ± 0.118	0.234 ± 0.155	0.131 ± 0.090
	05-28-10	None	0.004 ± 0.098	0.019 ± 0.089	0.019 ± 0.088	0.083 ± 0.117	0.085 ± 0.107	0.082 ± 0.090
		Rock	0.040 ± 0.112	0.059 ± 0.143	0.281 ± 0.210	0.131 ± 0.172	0.173 ± 0.152	0.487 ± 0.171
		Flap-Rock	0.003 ± 0.129	0.119 ± 0.108	0.189 ± 0.153	0.088 ± 0.062	0.134 ± 0.121	0.333 ± 0.187
	06-01-10	None	0.024 ± 0.117	0.017 ± 0.103	0.034 ± 0.097	0.093 ± 0.115	0.092 ± 0.095	0.088 ± 0.089
		Rock	0.000 ± 0.072	0.147 ± 0.165	0.485 ± 0.277	0.112 ± 0.134	0.305 ± 0.159	0.575 ± 0.182
		Flap	0.032 ± 0.101	0.051 ± 0.101	0.072 ± 0.120	0.101 ± 0.117	0.102 ± 0.096	0.093 ± 0.098
		Flap-Rock	0.133 ± 0.167	0.103 ± 0.137	0.359 ± 0.243	0.232 ± 0.171	0.285 ± 0.173	0.539 ± 0.166
2	01-18-08	None	0.048 ± 0.113	0.010 ± 0.090	0.022 ± 0.107	0.105 ± 0.101	0.115 ± 0.122	0.100 ± 0.096
		Flap	0.037 ± 0.134	0.058 ± 0.104	0.043 ± 0.094	0.084 ± 0.093	0.105 ± 0.138	0.119 ± 0.133
	01-24-08	None	0.054 ± 0.112	0.028 ± 0.103	0.053 ± 0.118	0.092 ± 0.098	0.109 ± 0.107	0.092 ± 0.112
		Rock	0.000 ± 0.000	0.014 ± 0.110	0.095 ± 0.088	0.000 ± 0.084	0.187 ± 0.121	0.174 ± 0.170
		Flap	0.039 ± 0.121	0.024 ± 0.088	0.076 ± 0.130	0.124 ± 0.113	0.173 ± 0.118	0.068 ± 0.060
	06-04-10	None	0.000 ± 0.103	0.003 ± 0.094	0.018 ± 0.106	0.080 ± 0.107	0.094 ± 0.110	0.081 ± 0.091
		Rock	0.000 ± 0.153	0.016 ± 0.167	0.191 ± 0.256	0.108 ± 0.156	0.103 ± 0.159	0.268 ± 0.218
		Flap	0.000 ± 0.065	0.148 ± 0.057	0.016 ± 0.064	0.042 ± 0.050	0.088 ± 0.080	0.042 ± 0.080
		Flap-Rock	0.000 ± 0.207	0.000 ± 0.025	0.050 ± 0.127	0.068 ± 0.079	0.059 ± 0.153	0.153 ± 0.264
	06-02-11	None	0.000 ± 0.099	0.000 ± 0.092	0.006 ± 0.110	0.085 ± 0.136	0.078 ± 0.125	0.098 ± 0.104
		Rock	0.000 ± 0.094	0.000 ± 0.110	0.000 ± 0.098	0.068 ± 0.129	0.097 ± 0.113	0.073 ± 0.084
3	01-18-08	None	0.003 ± 0.096	0.013 ± 0.114	0.016 ± 0.120	0.097 ± 0.108	0.087 ± 0.101	0.082 ± 0.091
		Flap	0.033 ± 0.043	0.023 ± 0.047	0.018 ± 0.060	0.127 ± 0.066	0.099 ± 0.048	0.075 ± 0.065
		Flap-Rock	0.060 ± 0.086	0.067 ± 0.149	0.064 ± 0.119	0.165 ± 0.147	0.214 ± 0.151	0.213 ± 0.179
	02-08-08	None	0.014 ± 0.106	0.035 ± 0.098	0.032 ± 0.082	0.096 ± 0.091	0.093 ± 0.098	0.093 ± 0.088
		Flap	0.048 ± 0.105	0.057 ± 0.103	0.062 ± 0.088	0.171 ± 0.132	0.161 ± 0.073	0.068 ± 0.064
		Flap-Rock	0.026 ± 0.089	0.037 ± 0.138	0.038 ± 0.116	0.116 ± 0.109	0.097 ± 0.078	0.149 ± 0.085

Supplementary Table S6. Pose Landmarks Median ± SD PS_1 Scores per Sensor, Stratified by Participant, Session, and Annotation Part II

Participant	Session	Annotation	RWrist	LWrist	Chest	RWrist Accel	LWrist Accel	Chest Accel
4	01-17-08	None	0.039 ± 0.100	0.051 ± 0.106	0.049 ± 0.112	0.114 ± 0.095	0.104 ± 0.105	0.102 ± 0.109
		Rock	0.107 ± 0.144	0.150 ± 0.163	0.221 ± 0.209	0.146 ± 0.114	0.194 ± 0.128	0.368 ± 0.164
		Flap	0.098 ± 0.127	0.071 ± 0.124	0.084 ± 0.136	0.128 ± 0.092	0.097 ± 0.089	0.089 ± 0.079
	02-07-08	None	0.048 ± 0.102	0.033 ± 0.115	0.041 ± 0.111	0.102 ± 0.086	0.099 ± 0.111	0.093 ± 0.083
		Rock	0.143 ± 0.166	0.104 ± 0.144	0.320 ± 0.224	0.185 ± 0.146	0.137 ± 0.122	0.325 ± 0.160
		Flap	0.055 ± 0.111	0.053 ± 0.106	0.070 ± 0.114	0.102 ± 0.102	0.145 ± 0.115	0.085 ± 0.093
	04-27-10	None	0.039 ± 0.104	0.010 ± 0.087	0.050 ± 0.106	0.092 ± 0.089	0.103 ± 0.103	0.089 ± 0.082
		Rock	0.468 ± 0.242	0.191 ± 0.171	0.688 ± 0.224	0.362 ± 0.162	0.191 ± 0.122	0.393 ± 0.170
		Flap	0.086 ± 0.069	0.121 ± 0.190	0.083 ± 0.089	0.080 ± 0.051	0.051 ± 0.086	0.086 ± 0.056
	05-11-10	None	0.022 ± 0.102	0.034 ± 0.097	0.042 ± 0.106	0.094 ± 0.094	0.094 ± 0.096	0.087 ± 0.091
		Rock	0.177 ± 0.182	0.116 ± 0.157	0.529 ± 0.242	0.121 ± 0.109	0.198 ± 0.137	0.307 ± 0.179
		Flap	0.047 ± 0.121	0.072 ± 0.086	0.086 ± 0.081	0.107 ± 0.143	0.116 ± 0.085	0.097 ± 0.079
5	01-16-08	None	0.039 ± 0.112	0.042 ± 0.099	0.022 ± 0.096	0.120 ± 0.113	0.106 ± 0.099	0.082 ± 0.088
		Rock	0.008 ± 0.120	0.120 ± 0.191	0.119 ± 0.198	0.045 ± 0.081	0.136 ± 0.124	0.055 ± 0.153
		Flap	0.012 ± 0.130	0.019 ± 0.126	0.021 ± 0.122	0.088 ± 0.134	0.100 ± 0.109	0.084 ± 0.088
		Flap-Rock	0.000 ± 0.076	0.000 ± 0.113	0.269 ± 0.216	0.108 ± 0.103	0.083 ± 0.087	0.190 ± 0.201
	02-08-08	None	0.026 ± 0.095	0.034 ± 0.115	0.042 ± 0.102	0.104 ± 0.118	0.113 ± 0.113	0.098 ± 0.094
		Flap	0.000 ± 0.098	0.050 ± 0.105	0.039 ± 0.101	0.119 ± 0.131	0.104 ± 0.096	0.096 ± 0.103
	05-17-10	None	0.000 ± 0.101	0.062 ± 0.117	0.058 ± 0.133	0.091 ± 0.127	0.119 ± 0.121	0.106 ± 0.117
		Rock	0.000 ± 0.116	0.070 ± 0.141	0.423 ± 0.217	0.076 ± 0.131	0.150 ± 0.144	0.439 ± 0.151
		Flap	0.019 ± 0.114	0.000 ± 0.095	0.081 ± 0.096	0.138 ± 0.137	0.110 ± 0.131	0.164 ± 0.102
		Flap-Rock	0.054 ± 0.071	0.291 ± 0.143	0.323 ± 0.172	0.073 ± 0.031	0.325 ± 0.075	0.225 ± 0.046
	05-25-11	None	0.035 ± 0.100	0.000 ± 0.072	0.035 ± 0.109	0.113 ± 0.118	0.115 ± 0.118	0.119 ± 0.105
		Rock	0.085 ± 0.095	0.067 ± 0.093	0.000 ± 0.119	0.082 ± 0.079	0.093 ± 0.076	0.115 ± 0.135
6	01-15-08	None	0.024 ± 0.106	0.022 ± 0.100	0.026 ± 0.113	0.116 ± 0.117	0.102 ± 0.124	0.109 ± 0.100
		Rock	0.061 ± 0.161	0.070 ± 0.175	0.422 ± 0.241	0.162 ± 0.167	0.181 ± 0.160	0.408 ± 0.203
		Flap-Rock	0.000 ± 0.108	0.000 ± 0.149	0.498 ± 0.247	0.079 ± 0.160	0.133 ± 0.194	0.508 ± 0.203
	01-23-08	None	0.054 ± 0.111	0.044 ± 0.103	0.040 ± 0.112	0.105 ± 0.106	0.105 ± 0.106	0.098 ± 0.103
		Rock	0.118 ± 0.200	0.092 ± 0.180	0.480 ± 0.258	0.194 ± 0.156	0.177 ± 0.170	0.464 ± 0.205
	03-12-10	None	0.002 ± 0.096	0.000 ± 0.079	0.061 ± 0.135	0.088 ± 0.108	0.065 ± 0.105	0.083 ± 0.105
		Rock	0.000 ± 0.133	0.000 ± 0.110	0.608 ± 0.220	0.065 ± 0.159	0.041 ± 0.137	0.456 ± 0.207
		Flap-Rock	0.051 ± 0.093	0.000 ± 0.087	0.025 ± 0.169	0.203 ± 0.163	0.089 ± 0.093	0.426 ± 0.217

Supplementary Table S7. Accelerometer Median ± SD PS_1 Scores per Sensor, Stratified by Child, Session, and Annotation Part I

Participant	Session	Annotation	Torso	LWrist	RWrist
1	01-18-08	None	0.000 ± 0.088	0.000 ± 0.042	0.000 ± 0.058
		Rock	0.265 ± 0.314	0.000 ± 0.107	0.000 ± 0.129
		Flap	0.019 ± 0.027	0.022 ± 0.011	0.125 ± 0.157
		Flap-Rock	0.324 ± 0.178	0.378 ± 0.179	0.413 ± 0.193
	01-25-08	None	0.000 ± 0.035	0.000 ± 0.031	0.000 ± 0.058
		Rock	0.380 ± 0.287	0.014 ± 0.209	0.009 ± 0.237
		Flap	0.017 ± 0.070	0.017 ± 0.167	0.574 ± 0.197
		Flap-Rock	0.115 ± 0.196	0.124 ± 0.173	0.134 ± 0.140
	05-25-10	None	0.000 ± 0.089	0.000 ± 0.101	0.000 ± 0.060
		Rock	0.642 ± 0.286	0.605 ± 0.283	0.000 ± 0.231
		Flap-Rock	0.459 ± 0.200	0.590 ± 0.186	0.589 ± 0.170
	05-28-10	None	0.000 ± 0.090	0.000 ± 0.101	0.000 ± 0.061
		Rock	0.633 ± 0.288	0.603 ± 0.284	0.000 ± 0.232
		Flap-Rock	0.462 ± 0.199	0.589 ± 0.184	0.591 ± 0.171
	06-01-10	None	0.000 ± 0.048	0.000 ± 0.051	0.000 ± 0.068
		Rock	0.474 ± 0.320	0.510 ± 0.271	0.000 ± 0.169
		Flap	0.080 ± 0.131	0.042 ± 0.104	0.164 ± 0.179
		Flap-Rock	0.718 ± 0.296	0.617 ± 0.278	0.175 ± 0.193
2	01-18-08	None	0.003 ± 0.017	0.000 ± 0.023	0.000 ± 0.017
		Flap	0.013 ± 0.033	0.078 ± 0.088	0.031 ± 0.061
	01-24-08	None	0.005 ± 0.026	0.000 ± 0.026	0.003 ± 0.049
		Rock	0.067 ± 0.240	0.050 ± 0.129	0.016 ± 0.127
		Flap	0.050 ± 0.045	0.047 ± 0.090	0.126 ± 0.083
	06-04-10	None	0.000 ± 0.053	0.000 ± 0.044	0.000 ± 0.089
		Rock	0.411 ± 0.244	0.095 ± 0.246	0.104 ± 0.189
		Flap	0.000 ± 0.003	0.000 ± 0.012	0.008 ± 0.008
		Flap-Rock	0.490 ± 0.225	0.000 ± 0.187	0.084 ± 0.169
	06-02-11	None	0.010 ± 0.101	0.004 ± 0.088	0.004 ± 0.074
		Rock	0.000 ± 0.086	0.000 ± 0.064	0.000 ± 0.059
3	01-18-08	None	0.000 ± 0.021	0.000 ± 0.035	0.000 ± 0.020
		Flap	0.000 ± 0.051	0.012 ± 0.029	0.015 ± 0.181
		Flap-Rock	0.356 ± 0.177	0.234 ± 0.164	0.343 ± 0.147
	02-08-08	None	0.000 ± 0.022	0.000 ± 0.025	0.000 ± 0.016
		Flap	0.019 ± 0.056	0.024 ± 0.047	0.000 ± 0.062
		Flap-Rock	0.537 ± 0.181	0.237 ± 0.165	0.400 ± 0.159

Supplementary Table S8. Accelerometer Median ± SD PS_1 Scores per Sensor, Stratified by Child, Session, and Annotation Part II

Participant	Session	Annotation	Torso	LWrist	RWrist
4	01-17-08	None	0.000 ± 0.050	0.000 ± 0.031	0.000 ± 0.048
		Rock	0.619 ± 0.196	0.000 ± 0.115	0.000 ± 0.086
		Flap	0.093 ± 0.084	0.016 ± 0.049	0.014 ± 0.047
	02-07-08	None	0.000 ± 0.051	0.000 ± 0.029	0.002 ± 0.045
		Rock	0.585 ± 0.220	0.000 ± 0.159	0.000 ± 0.116
		Flap	0.058 ± 0.072	0.013 ± 0.036	0.011 ± 0.041
	04-27-10	None	0.000 ± 0.036	0.000 ± 0.026	0.000 ± 0.059
		Rock	0.690 ± 0.221	0.000 ± 0.239	0.000 ± 0.089
		Flap	0.122 ± 0.055	0.078 ± 0.090	0.095 ± 0.092
	05-11-10	None	0.000 ± 0.067	0.000 ± 0.041	0.000 ± 0.050
		Rock	0.641 ± 0.255	0.000 ± 0.190	0.000 ± 0.115
		Flap	0.081 ± 0.067	0.037 ± 0.100	0.083 ± 0.123
5	01-16-08	None	0.000 ± 0.073	0.000 ± 0.046	0.000 ± 0.090
		Rock	0.014 ± 0.238	0.000 ± 0.170	0.001 ± 0.193
		Flap	0.000 ± 0.103	0.045 ± 0.070	0.037 ± 0.063
		Flap-Rock	0.298 ± 0.177	0.049 ± 0.051	0.047 ± 0.064
	02-08-08	None	0.002 ± 0.016	0.003 ± 0.028	0.003 ± 0.020
		Flap	0.016 ± 0.040	0.106 ± 0.119	0.013 ± 0.069
	05-17-10	None	0.006 ± 0.102	0.020 ± 0.082	0.009 ± 0.108
		Rock	0.226 ± 0.341	0.000 ± 0.189	0.000 ± 0.178
		Flap	0.030 ± 0.126	0.021 ± 0.085	0.020 ± 0.120
		Flap-Rock	0.467 ± 0.242	0.359 ± 0.300	0.187 ± 0.058
	05-25-11	None	0.000 ± 0.020	0.003 ± 0.016	0.000 ± 0.022
		Rock	0.000 ± 0.077	0.000 ± 0.000	0.000 ± 0.013
6	01-15-08	None	0.000 ± 0.015	0.000 ± 0.022	0.000 ± 0.016
		Rock	0.499 ± 0.249	0.037 ± 0.181	0.000 ± 0.174
		Flap-Rock	0.563 ± 0.209	0.113 ± 0.146	0.075 ± 0.125
	01-23-08	None	0.000 ± 0.011	0.000 ± 0.016	0.000 ± 0.014
		Rock	0.537 ± 0.278	0.000 ± 0.169	0.000 ± 0.138
	03-12-10	None	0.005 ± 0.126	0.002 ± 0.094	0.000 ± 0.054
		Rock	0.461 ± 0.224	0.290 ± 0.208	0.279 ± 0.215
		Flap-Rock	0.295 ± 0.207	0.279 ± 0.174	0.118 ± 0.112

Estimated Period Summary Across Participants, Sessions, and Annotations

Supplementary Table S9. Pose Landmarks Median[IQR] Period Estimation per Sensor, Stratified by Child, Session, and Annotation Part I

Participant	Session	Annotation	L Wrist	R Wrist	Chest	L Wrist Accel	R Wrist Accel	Chest Accel
1	01-18-08	None	4.000[2.000~4.000]	4.000[2.000~4.000]	4.000[2.000~4.000]	1.000[0.800~1.333]	1.333[1.000~2.000]	1.000[0.800~1.333]
		Rock	2.000[2.000~4.000]	4.000[2.000~4.000]	2.000[2.000~4.000]	1.333[0.950~2.000]	1.333[1.000~2.000]	1.000[0.800~1.333]
		Flap	4.000[4.000~4.000]	4.000[2.500~4.000]	4.000[2.500~4.000]	0.733[0.667~0.800]	0.800[0.800~0.800]	0.900[0.800~1.750]
		Flap-Rock	2.000[2.000~4.000]	4.000[2.000~4.000]	2.000[2.000~4.000]	0.800[0.667~1.333]	1.000[0.800~2.000]	0.667[0.500~0.800]
	01-25-08	None	4.000[2.000~4.000]	4.000[2.000~4.000]	4.000[2.000~4.000]	0.800[0.571~1.000]	1.000[0.800~1.333]	0.800[0.571~1.000]
		Rock	2.000[1.333~4.000]	2.000[1.333~4.000]	2.000[1.333~4.000]	1.333[0.800~1.333]	1.333[1.000~1.333]	1.333[0.800~1.333]
		Flap	2.000[1.333~4.000]	4.000[2.000~4.000]	2.000[0.667~4.000]	0.571[0.571~0.667]	2.000[2.000~4.000]	0.667[0.571~0.667]
		Flap-Rock	2.000[1.333~4.000]	4.000[2.000~4.000]	4.000[2.000~4.000]	1.000[0.800~1.333]	1.000[0.667~1.333]	0.667[0.500~1.000]
	05-25-10	None	4.000[2.000~4.000]	4.000[2.000~4.000]	4.000[2.000~4.000]	1.000[0.667~1.333]	0.800[0.667~1.333]	0.800[0.571~1.333]
		Rock	2.000[1.000~4.000]	2.000[1.000~4.000]	1.000[1.000~1.333]	1.000[1.000~1.000]	1.000[0.571~1.000]	1.000[1.000~1.000]
		Flap-Rock	2.000[2.000~4.000]	2.000[2.000~4.000]	2.000[2.000~4.000]	0.571[0.400~1.000]	0.571[0.444~1.333]	0.500[0.500~0.667]
	05-28-10	None	4.000[2.000~4.000]	4.000[2.000~4.000]	4.000[2.000~4.000]	1.000[0.733~1.333]	1.333[0.800~2.000]	0.800[0.571~1.333]
		Rock	4.000[1.333~4.000]	2.000[2.000~4.000]	1.000[1.000~2.000]	1.000[1.000~1.000]	1.333[1.000~2.000]	1.000[1.000~1.000]
		Flap-Rock	2.000[2.000~2.000]	2.000[2.000~4.000]	1.000[1.000~1.833]	1.333[1.000~2.000]	2.000[1.000~2.000]	1.000[0.800~1.000]
	06-01-10	None	4.000[2.000~4.000]	4.000[2.000~4.000]	4.000[2.000~4.000]	1.000[0.667~1.333]	1.000[0.800~1.333]	0.800[0.667~1.333]
		Rock	2.000[1.000~4.000]	4.000[2.000~4.000]	1.000[1.000~2.000]	1.000[1.000~1.000]	1.333[1.000~2.000]	1.000[1.000~1.000]
		Flap	4.000[2.000~4.000]	4.000[2.000~4.000]	4.000[2.000~4.000]	0.800[0.667~1.000]	0.800[0.571~1.000]	0.800[0.571~1.000]
		Flap-Rock	2.000[1.000~4.000]	2.000[1.000~4.000]	1.000[0.800~1.000]	1.000[0.800~1.000]	1.000[0.800~1.000]	1.000[0.800~1.000]
2	01-18-08	None	4.000[2.000~4.000]	4.000[2.000~4.000]	4.000[2.000~4.000]	1.333[1.000~1.333]	1.000[0.800~1.333]	1.000[0.800~1.333]
		Flap	2.000[2.000~4.000]	4.000[2.000~4.000]	4.000[2.000~4.000]	1.333[1.000~2.000]	1.333[1.333~2.000]	1.000[0.667~1.167]
	01-24-08	None	4.000[2.000~4.000]	4.000[2.000~4.000]	4.000[2.000~4.000]	1.333[0.800~1.333]	0.800[0.667~1.333]	0.800[0.667~1.333]
		Rock	2.000[2.000~4.000]	4.000[4.000~4.000]	2.000[2.000~2.000]	1.000[0.800~1.333]	4.000[4.000~4.000]	2.000[1.833~2.000]
		Flap	2.000[1.333~4.000]	4.000[2.000~4.000]	2.000[2.000~4.000]	1.333[1.000~2.000]	1.000[0.800~1.333]	0.667[0.571~0.800]
	06-04-10	None	4.000[2.000~4.000]	4.000[2.000~4.000]	4.000[2.000~4.000]	1.000[0.667~2.000]	1.000[0.667~2.000]	0.800[0.571~1.333]
		Rock	2.000[1.333~4.000]	4.000[2.000~4.000]	1.333[1.333~4.000]	1.333[1.333~2.000]	1.333[0.800~2.000]	1.333[1.333~2.000]
		Flap	2.000[2.000~4.000]	2.000[2.000~2.000]	2.000[2.000~2.000]	1.333[1.000~1.333]	2.000[2.000~2.000]	0.444[0.400~0.686]
		Flap-Rock	4.000[2.000~4.000]	4.000[2.000~4.000]	4.000[3.500~4.000]	2.000[2.000~2.000]	2.000[2.000~2.000]	2.000[1.833~2.000]
	06-02-11	None	4.000[4.000~4.000]	4.000[4.000~4.000]	4.000[2.000~4.000]	1.333[0.800~2.000]	1.333[0.667~2.000]	1.000[0.800~1.333]
		Rock	4.000[2.000~4.000]	4.000[4.000~4.000]	4.000[2.000~4.000]	1.333[0.800~2.000]	1.333[0.800~2.000]	2.000[1.000~2.000]
3	01-18-08	None	4.000[4.000~4.000]	4.000[2.000~4.000]	4.000[2.000~4.000]	1.000[0.800~1.333]	1.000[0.800~1.333]	1.000[0.800~1.333]
		Flap	4.000[2.000~4.000]	4.000[2.000~4.000]	4.000[3.500~4.000]	1.000[0.800~1.333]	1.000[0.800~1.083]	1.000[1.000~1.333]
		Flap-Rock	2.000[2.000~4.000]	4.000[2.000~4.000]	4.000[2.000~4.000]	0.667[0.667~1.333]	1.000[0.667~1.333]	0.667[0.571~1.000]
	02-08-08	None	4.000[2.000~4.000]	4.000[2.000~4.000]	4.000[2.000~4.000]	1.000[0.667~1.333]	1.000[0.800~1.333]	0.800[0.667~1.333]
		Flap	4.000[4.000~4.000]	4.000[2.000~4.000]	4.000[4.000~4.000]	1.000[0.800~1.000]	1.000[1.000~1.333]	0.733[0.667~1.250]
		Flap-Rock	4.000[2.000~4.000]	4.000[2.000~4.000]	4.000[2.000~4.000]	0.800[0.667~1.333]	1.333[0.667~1.333]	0.571[0.500~0.667]

Supplementary Table S10. Pose Landmarks Median[IQR] Period Estimation per Sensor, Stratified by Child, Session, and Annotation Part II

Participant	Session	Annotation	L Wrist	R Wrist	Chest	L Wrist Accel	R Wrist Accel	Chest Accel
4	01-17-08	None	4.000[2.000~4.000]	4.000[2.000~4.000]	4.000[2.000~4.000]	1.000[0.667~1.333]	0.800[0.667~1.333]	0.800[0.667~1.000]
		Rock	1.333[1.333~4.000]	1.333[1.333~4.000]	1.333[1.333~2.000]	1.333[0.800~1.333]	1.333[1.000~1.333]	0.667[0.667~1.333]
		Flap	4.000[2.000~4.000]	4.000[2.000~4.000]	4.000[2.000~4.000]	1.000[0.667~1.000]	1.000[0.800~1.000]	0.800[0.667~1.000]
	02-07-08	None	4.000[2.000~4.000]	4.000[2.000~4.000]	4.000[2.000~4.000]	1.333[0.800~2.000]	1.000[0.667~1.333]	0.800[0.667~1.333]
		Rock	2.000[1.333~4.000]	2.000[1.333~2.000]	1.333[1.333~2.000]	0.800[0.667~1.333]	1.333[0.800~1.333]	0.800[0.667~1.333]
		Flap	4.000[2.000~4.000]	4.000[2.000~4.000]	2.000[2.000~4.000]	1.000[0.667~1.333]	1.000[0.800~1.333]	0.800[0.571~1.000]
	04-27-10	None	4.000[2.000~4.000]	4.000[2.000~4.000]	4.000[2.000~4.000]	0.667[0.500~1.000]	0.800[0.571~1.000]	0.800[0.571~1.000]
		Rock	1.333[1.333~2.000]	1.333[1.333~1.333]	1.333[1.333~1.333]	1.000[0.667~1.333]	1.333[1.333~1.333]	1.333[0.667~1.333]
		Flap	4.000[1.333~4.000]	2.000[2.000~4.000]	4.000[4.000~4.000]	0.800[0.667~1.333]	0.667[0.571~0.667]	0.500[0.444~0.667]
	05-11-10	None	4.000[2.000~4.000]	4.000[2.000~4.000]	4.000[2.000~4.000]	0.800[0.667~1.333]	1.000[0.667~1.333]	0.800[0.571~1.333]
		Rock	2.000[1.333~2.000]	1.333[1.333~2.000]	1.333[1.333~1.333]	0.800[0.667~1.000]	1.000[0.667~1.333]	0.800[0.667~1.333]
		Flap	2.000[2.000~4.000]	4.000[2.000~4.000]	4.000[2.000~4.000]	0.667[0.571~1.000]	1.000[0.800~1.333]	0.667[0.571~0.800]
5	01-16-08	None	4.000[2.000~4.000]	4.000[2.000~4.000]	4.000[2.000~4.000]	0.800[0.667~1.333]	0.800[0.667~1.333]	1.000[0.800~1.333]
		Rock	2.000[2.000~4.000]	4.000[2.000~4.000]	2.000[2.000~4.000]	1.333[1.000~1.333]	1.333[1.000~2.000]	2.000[1.333~2.000]
		Flap	4.000[2.000~4.000]	2.000[2.000~4.000]	4.000[2.000~4.000]	1.333[1.000~1.333]	1.333[1.000~1.333]	1.333[1.333~2.000]
		Flap-Rock	4.000[2.000~4.000]	4.000[2.000~4.000]	2.000[2.000~2.000]	2.000[1.333~2.000]	2.000[2.000~2.000]	1.333[1.333~2.000]
	02-08-08	None	4.000[2.000~4.000]	4.000[2.000~4.000]	4.000[2.000~4.000]	0.800[0.667~1.333]	0.800[0.571~1.000]	0.800[0.571~1.000]
		Flap	4.000[2.000~4.000]	4.000[4.000~4.000]	4.000[2.000~4.000]	1.000[0.800~1.333]	0.667[0.500~1.000]	0.667[0.571~1.000]
	05-17-10	None	2.000[2.000~4.000]	4.000[2.000~4.000]	4.000[2.000~4.000]	1.000[0.667~1.333]	1.333[0.800~2.000]	0.667[0.500~1.000]
		Rock	2.000[2.000~4.000]	4.000[2.000~4.000]	1.333[1.333~1.333]	1.333[1.000~1.333]	1.333[1.000~2.000]	1.333[1.000~1.333]
		Flap	4.000[2.000~4.000]	4.000[2.000~4.000]	2.000[2.000~4.000]	1.333[0.595~2.000]	1.000[0.667~1.333]	0.800[0.571~1.333]
		Flap-Rock	1.333[1.333~2.000]	1.333[1.333~4.000]	2.000[1.333~2.000]	1.333[1.000~1.333]	1.333[1.333~1.333]	1.333[1.333~1.333]
	05-25-11	None	4.000[4.000~4.000]	4.000[2.000~4.000]	4.000[2.000~4.000]	0.667[0.500~1.000]	0.800[0.571~1.333]	0.800[0.571~1.000]
		Rock	2.000[2.000~4.000]	4.000[2.000~4.000]	4.000[4.000~4.000]	1.000[0.800~1.333]	1.167[0.571~1.333]	2.000[1.333~2.000]
6	01-15-08	None	4.000[2.000~4.000]	4.000[2.000~4.000]	4.000[2.000~4.000]	1.000[0.800~1.333]	1.000[0.667~1.333]	1.000[0.667~1.333]
		Rock	2.000[1.333~4.000]	2.000[1.333~4.000]	1.333[1.333~2.000]	1.333[1.333~1.333]	1.333[1.000~1.333]	1.333[1.333~1.333]
		Flap-Rock	2.000[2.000~4.000]	4.000[2.000~4.000]	1.333[1.000~2.000]	2.000[1.333~2.000]	1.333[1.333~2.000]	1.000[1.000~1.333]
	01-23-08	None	4.000[2.000~4.000]	4.000[2.000~4.000]	4.000[2.000~4.000]	0.800[0.571~1.333]	0.800[0.571~1.000]	1.000[0.800~1.333]
		Rock	2.000[1.333~4.000]	2.000[1.333~4.000]	1.333[1.333~1.333]	1.333[1.333~1.333]	1.333[1.333~1.333]	1.333[1.333~1.333]
	03-12-10	None	4.000[2.000~4.000]	4.000[2.000~4.000]	4.000[2.000~4.000]	1.333[0.800~2.000]	1.000[0.800~1.333]	0.800[0.571~1.333]
		Rock	4.000[2.000~4.000]	4.000[2.000~4.000]	1.333[1.333~1.333]	2.000[1.333~4.000]	2.000[1.333~2.000]	1.333[1.333~1.333]
		Flap-Rock	4.000[2.000~4.000]	4.000[2.000~4.000]	4.000[1.000~4.000]	1.333[0.458~2.000]	0.667[0.500~1.000]	0.571[0.500~0.800]

Supplementary Table S11. Accelerometer Median[IQR] Period Estimation per Sensor, Stratified by Child, Session, and Annotation Part I

Participant	Session	Annotation	Torso	L Wrist	R Wrist
1	01-18-08	None	3.700 [3.690–3.700]	3.700 [3.100–3.700]	3.690 [3.100–3.700]
		Rock	1.700 [1.298–3.690]	3.690 [2.896–3.700]	2.900 [1.302–3.700]
		Flap	3.700 [3.700–3.700]	3.690 [3.690–3.690]	1.097 [1.097–1.097]
		Flap-Rock	1.297 [1.100–1.700]	1.297 [1.100–1.300]	1.297 [1.100–1.300]
	01-25-08	None	3.700 [3.690–3.700]	3.700 [3.690–3.700]	3.700 [3.681–3.700]
		Rock	1.696 [1.298–3.690]	1.704 [1.300–3.700]	2.908 [1.298–3.700]
		Flap	3.695 [3.693–3.698]	3.700 [3.700–3.700]	2.390 [1.745–3.035]
		Flap-Rock	1.696 [1.300–3.104]	1.100 [1.099–1.302]	1.103 [1.100–1.300]
	05-25-10	None	3.700 [3.700–3.707]	3.700 [3.100–3.710]	3.700 [3.108–3.700]
		Rock	1.103 [1.100–1.201]	1.100 [1.100–1.103]	3.700 [1.201–3.705]
		Flap-Rock	1.103 [1.100–1.303]	1.103 [1.100–1.300]	1.100 [0.900–1.300]
	05-28-10	None	3.700 [3.700–3.700]	3.700 [3.100–3.710]	3.700 [3.108–3.700]
		Rock	1.100 [1.100–1.251]	1.100 [1.100–1.103]	3.700 [1.152–3.700]
		Flap-Rock	1.103 [1.100–1.300]	1.103 [1.100–1.300]	1.100 [0.900–1.300]
	06-01-10	None	3.700 [3.700–3.710]	3.700 [3.100–3.700]	3.700 [3.100–3.707]
		Rock	1.101 [1.100–1.103]	1.101 [1.100–1.103]	3.400 [2.651–3.700]
		Flap	3.700 [3.700–3.710]	3.700 [2.900–3.700]	1.700 [1.103–3.700]
		Flap-Rock	1.100 [1.100–1.700]	1.103 [1.100–1.700]	1.103 [0.900–1.300]
2	01-18-08	None	3.700 [3.690–3.700]	3.690 [3.092–3.700]	3.700 [3.690–3.700]
		Flap	3.700 [3.700–3.700]	1.297 [1.097–1.300]	3.690 [1.300–3.710]
	01-24-08	None	3.700 [3.690–3.700]	3.100 [2.894–3.700]	3.695 [3.690–3.700]
		Rock	1.803 [1.552–2.055]	1.797 [1.548–2.045]	1.795 [1.546–2.045]
		Flap	3.700 [3.690–3.702]	1.200 [1.099–1.403]	1.200 [1.000–2.000]
	06-04-10	None	3.700 [3.100–3.700]	3.108 [2.200–3.700]	3.004 [2.300–3.700]
		Rock	1.302 [1.251–1.700]	1.700 [1.303–2.451]	1.802 [1.300–2.956]
		Flap	3.700 [3.700–3.700]	3.705 [3.702–3.707]	2.000 [1.850–2.150]
		Flap-Rock	1.700 [1.700–1.700]	2.700 [2.200–3.200]	1.500 [1.400–1.600]
	06-02-11	None	2.908 [1.700–3.700]	2.306 [1.303–3.108]	2.303 [1.300–3.698]
		Rock	2.306 [2.300–2.900]	2.306 [2.300–2.908]	2.306 [1.992–2.906]
3	01-18-08	None	3.700 [3.690–3.700]	3.690 [3.614–3.700]	3.700 [3.690–3.700]
		Flap	3.700 [3.690–3.700]	3.100 [1.097–3.690]	1.300 [1.201–3.399]
		Flap-Rock	1.198 [1.098–1.303]	1.198 [1.100–1.299]	1.200 [1.100–1.297]
	02-08-08	None	3.700 [3.690–3.700]	3.700 [3.690–3.700]	3.700 [3.690–3.700]
		Flap	3.700 [3.690–3.700]	3.092 [3.092–3.096]	3.100 [3.000–3.695]
		Flap-Rock	1.200 [1.100–1.297]	1.100 [1.100–1.297]	1.300 [1.100–1.401]

Supplementary Table S12. Accelerometer Median[IQR] Period Estimation per Sensor, Stratified by Child, Session, and Annotation Part II

Participant	Session	Annotation	Torso	L Wrist	R Wrist
4	01-17-08	None	3.700 [3.690–3.700]	3.690 [3.635–3.700]	3.700 [3.690–3.700]
		Rock	1.300 [1.300–1.300]	3.700 [3.681–3.700]	3.700 [3.690–3.700]
		Flap	3.700 [3.690–3.700]	2.300 [1.300–2.908]	2.294 [1.300–2.900]
	02-07-08	None	3.690 [3.102–3.700]	3.690 [2.944–3.700]	3.700 [3.100–3.700]
		Rock	1.300 [1.297–1.696]	3.690 [3.092–3.700]	3.700 [3.102–3.700]
		Flap	3.700 [3.690–3.700]	1.700 [1.293–2.900]	2.093 [1.297–2.898]
	04-27-10	None	3.700 [3.700–3.710]	3.108 [2.271–3.700]	3.700 [2.904–3.700]
		Rock	1.300 [1.300–1.303]	1.504 [1.303–3.700]	3.700 [3.100–3.710]
		Flap	3.100 [3.100–3.104]	2.900 [2.600–2.900]	2.300 [1.701–2.600]
	05-11-10	None	3.700 [3.700–3.710]	3.700 [3.108–3.710]	3.700 [3.100–3.700]
		Rock	1.300 [1.300–1.696]	3.700 [1.700–3.700]	3.700 [2.908–3.700]
		Flap	3.700 [3.700–3.700]	1.300 [1.100–2.400]	1.300 [1.300–2.002]
5	01-16-08	None	3.700 [3.690–3.700]	3.690 [3.647–3.700]	3.700 [3.690–3.700]
		Rock	2.103 [1.700–2.948]	3.381 [2.200–3.690]	3.000 [1.850–3.683]
		Flap	3.690 [3.690–3.700]	1.696 [1.297–1.700]	1.303 [1.300–2.306]
		Flap-Rock	1.700 [1.694–1.704]	1.698 [1.299–1.700]	1.700 [1.597–1.700]
	02-08-08	None	3.700 [3.690–3.700]	3.700 [3.690–3.700]	3.700 [3.690–3.700]
		Flap	3.700 [3.700–3.700]	1.700 [1.100–3.690]	3.700 [3.690–3.700]
	05-17-10	None	3.700 [3.700–3.700]	3.700 [3.700–3.710]	3.700 [3.690–3.705]
		Rock	1.303 [1.103–3.700]	3.700 [3.100–3.710]	3.700 [2.885–3.700]
		Flap	3.700 [3.698–3.700]	3.104 [1.904–3.700]	3.681 [1.702–3.710]
		Flap-Rock	1.704 [1.704–1.704]	1.700 [1.700–1.700]	1.700 [1.700–1.700]
	05-25-11	None	3.705 [3.700–3.710]	3.710 [3.700–3.710]	3.710 [3.700–3.710]
		Rock	3.400 [2.950–3.700]	3.700 [3.529–3.700]	3.572 [3.041–3.695]
6	01-15-08	None	3.700 [3.690–3.700]	3.690 [3.681–3.700]	3.700 [3.690–3.700]
		Rock	1.300 [1.103–1.303]	2.300 [1.297–3.688]	3.700 [2.900–3.700]
		Flap-Rock	1.103 [1.100–1.300]	1.103 [1.097–1.300]	1.103 [1.100–1.303]
	01-23-08	None	3.700 [3.700–3.700]	3.690 [3.690–3.700]	3.700 [3.690–3.700]
		Rock	1.300 [1.297–1.303]	3.092 [1.303–3.690]	3.700 [3.690–3.700]
	03-12-10	None	3.700 [3.700–3.710]	3.700 [3.100–3.710]	3.359 [2.908–3.700]
		Rock	1.300 [1.300–1.303]	1.300 [1.278–1.303]	1.300 [1.278–1.303]
		Flap-Rock	1.101 [0.800–1.251]	1.100 [0.801–1.253]	1.300 [1.150–1.303]

Supplementary Note 8. Comparison to Spectral Methods

Given a point cloud $X = \{x_1, \ldots, x_n\} \subset \mathbb{R}^D$ arising from the sliding window embedding, we construct a weighted ε-neighborhood graph $G_\varepsilon = (V, E)$ as follows. Each vertex corresponds to a point $x_i \in X$, and edges are defined by

$$(i, j) \in E \quad \Longleftrightarrow \quad \|x_i - x_j\| \leq \varepsilon.$$

We assign weights using a Gaussian kernel,

$$w_{ij} = \exp\left(-\frac{\|x_i - x_j\|^2}{\sigma^2}\right),$$

where σ is chosen as the median of the nonzero pairwise distances.

The adjacency matrix $A \in \mathbb{R}^{n \times n}$ is defined by $A_{ij} = w_{ij}$ if $(i, j) \in E$ and $A_{ij} = 0$ otherwise. Let D denote the diagonal degree matrix with entries $D_{ii} = \sum_j A_{ij}$. The normalized graph Laplacian is then given by

$$L = I - D^{-1/2} A D^{-1/2}.$$

To select the neighborhood scale ε in a data-driven manner, we use the 0-dimensional persistence diagram Dgm_0 of the Vietoris–Rips filtration on X. Specifically, we define

$$\varepsilon^* = \max\{d : (b, d) \in \mathrm{Dgm}_0,\ d < \infty\},$$

which corresponds to the smallest radius at which the point cloud becomes connected. The graph Laplacian is then constructed using ε^*.

Finally, we compute the eigenvalues

$$0 = \lambda_1 \leq \lambda_2 \leq \cdots \leq \lambda_n$$

of L. The first k nontrivial eigenvalues $(\lambda_2, \ldots, \lambda_{k+1})$ are used as spectral features, while the associated eigenvectors define a k-dimensional subspace whose projection matrix

$$P = U_k U_k^\top$$

is used for computing chordal distances between sliding window embeddings in non-euclidean clustering analyses. This construction provides a manifold-learning-based baseline that captures geometric structure, in contrast to the proposed topological features derived from persistent homology.

We replicate experiment 1 with the eigenvalues from the Laplacian to show another method used on the sliding window point cloud. To ensure a fair comparison, we use the same Random Forest classifier and identical Bayesian hyperparameter optimization pipeline as in the SW1PerS experiments.

Supplementary Table S13. Classification performance of Random Forest models using normalized Laplacian eigenvalues.

	Pose Estimation			
Class	Precision	Recall	F1	Support
Binary Classification				
None	0.73	0.77	0.75	449
SMM	0.65	0.60	0.62	319
Weighted $F1$				**0.69**
Multiclass Classification				
None	0.69	0.62	0.66	449
Rock	0.57	0.64	0.60	259
Flap	0.06	0.09	0.07	43
Flap-Rock	0.00	0.00	0.00	17
Weighted $F1$				**0.33**

Supplementary Fig 21. Acceleration Distribution

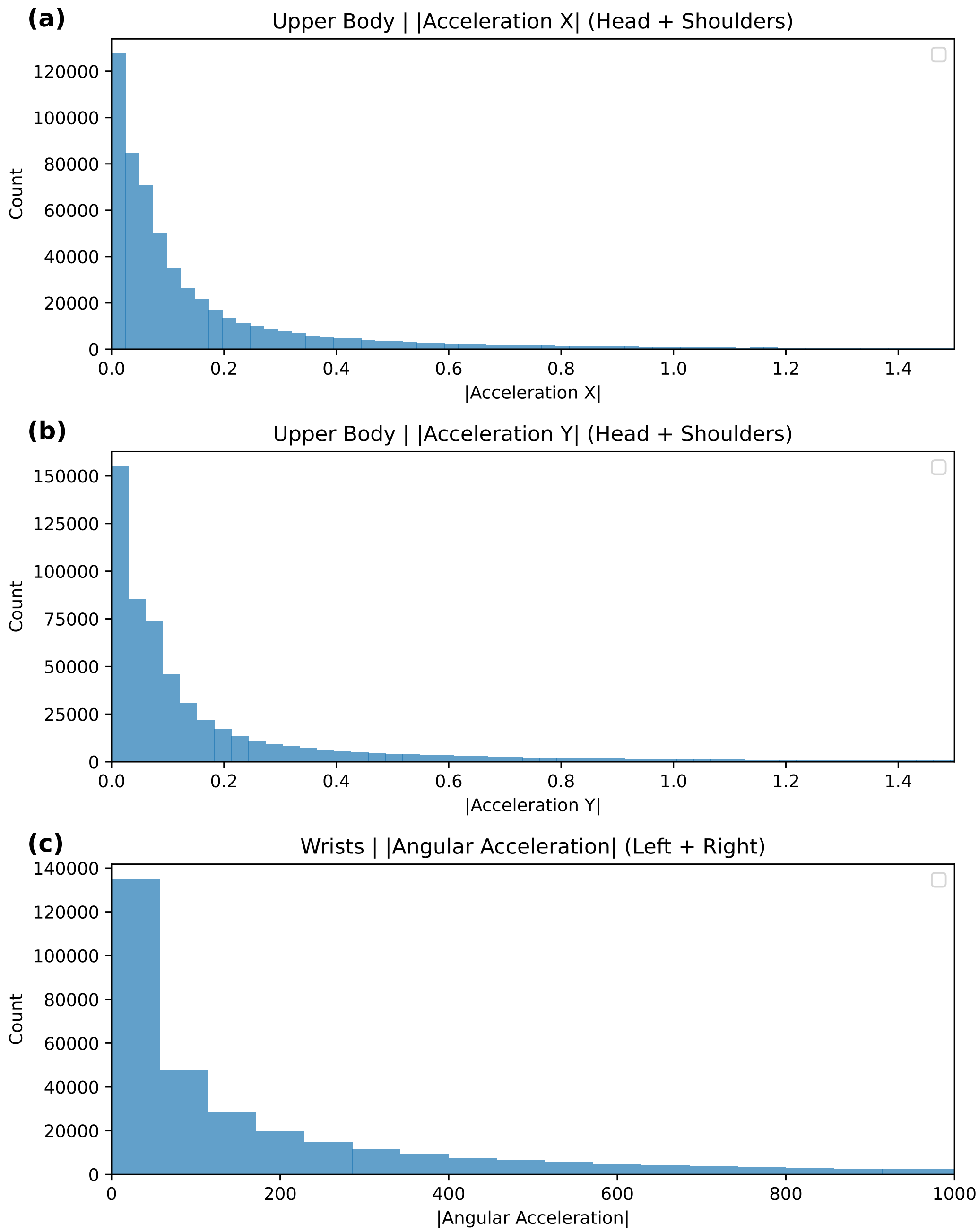

Supplementary Figure S23. Distribution of linear (**a,b**) and angular acceleration (**c**)magnitudes across all time segments and body locations. Both distributions exhibit heavy-tailed behavior, with the majority of values concentrated at low magnitudes and a small number of large outliers. This supports the selection of acceleration thresholds used for filtering unreliable frames, as thresholds near the upper tail remove high-amplitude noise while preserving the majority of the signal.

References

1. Lin, T.-Y. *et al.* Microsoft coco: Common objects in context (2015). 1405.0312.

2. Perea, J. A. & Harer, J. Sliding windows and persistence: An application of topological methods to signal analysis. *Foundations computational mathematics* **15**, 799–838 (2015).

3. Goodwin, M. S. *et al.* Moving towards a real-time system for automatically recognizing stereotypical motor movements in individuals on the autism spectrum using wireless accelerometry. In *Proceedings of the 2014 ACM International Joint Conference on Pervasive and Ubiquitous Computing*, UbiComp '14, 861–872, DOI: 10.1145/2632048.2632096 (Association for Computing Machinery, New York, NY, USA, 2014).

4. Zhang, L., Gorovits, A., Zhang, W. & Bogdanov, P. Learning periods from incomplete multivariate time series. In *2020 IEEE International Conference on Data Mining (ICDM)*, 1394–1399, DOI: 10.1109/ICDM50108.2020.00183 (2020).

5. Großekathöfer, U. *et al.* Automated detection of stereotypical motor movements in autism spectrum disorder using recurrence quantification analysis. *Front. neuroinformatics* **11**, 9 (2017).

6. Rad, N. M. *et al.* Convolutional neural network for stereotypical motor movement detection in autism. *arXiv preprint arXiv:1511.01865* (2015).

7. Sadouk, L., Gadi, T. & Essoufi, E. H. A novel deep learning approach for recognizing stereotypical motor movements within and across subjects on the autism spectrum disorder. *Comput. intelligence neuroscience* **2018**, 7186762 (2018).